SANDIA REPORT

SAND2003-3824
Unlimited Release
Printed October 2003

Investigation of Oil Injection into Brine for the Strategic Petroleum Reserve—Hydrodynamics Experiments with Simulant Liquids

Timothy J. O'Hern, John R. Torczynski, Jeremy Barney, Jaime Castañeda, Raymond O. Cote, Kim A. Shollenberger

Prepared by
Sandia National Laboratories
Albuquerque, New Mexico 87185 and Livermore, California 94550

Sandia is a multiprogram laboratory operated by Sandia Corporation, a Lockheed Martin Company, for the United States Department of Energy's National Nuclear Security Administration under Contract DE-AC04-94AL85000.

Issued by Sandia National Laboratories, operated for the United States Department of Energy by Sandia Corporation.

Available to DOE and DOE contractors from
U.S. Department of Energy
Office of Scientific and Technical Information
P.O. Box 62
Oak Ridge, TN 37831

Telephone: (865)576-8401
Facsimile: (865)576-5728
E-Mail: reports@adonis.osti.gov
Online ordering: http://www.doe.gov/bridge

Available to the public from
U.S. Department of Commerce
National Technical Information Service
5285 Port Royal Rd
Springfield, VA 22161

Telephone: (800)553-6847
Facsimile: (703)605-6900
E-Mail: orders@ntis.fedworld.gov
Online order: http://www.ntis.gov/help/ordermethods.asp?loc=7-4-0#online

SAND2003-3824
Unlimited Release
Printed October 2003

Investigation of Oil Injection into Brine for the Strategic Petroleum Reserve—Hydrodynamics Experiments with Simulant Liquids

Timothy J. O'Hern, John R. Torczynski, Jeremy Barney, Jaime N. Castañeda, Raymond O. Cote
Engineering Sciences Center
Sandia National Laboratories
P.O. Box 5800
Albuquerque, NM 87185-0834

Kim A. Shollenberger
Mechanical Engineering Department
California Polytechnic State University
San Luis Obispo, CA 93407

ABSTRACT

An experimental program is being conducted to study a proposed approach for oil reintroduction in the Strategic Petroleum Reserve (SPR). The goal is to assess whether useful oil is rendered unusable through formation of a stable oil-brine emulsion during reintroduction of degassed oil into the brine layer in storage caverns. This report documents the first stage of the program, in which simulant liquids are used to characterize the buoyant plume that is produced when a jet of crude oil is injected downward from a tube into brine.

The experiment consists of a large transparent vessel that is a scale model of the proposed oil-injection process at the SPR. An oil layer is floated on top of a brine layer. Silicon oil (Dow Corning 200® Fluid, 5 cSt) is used as the simulant for crude oil to allow visualization of the flow and to avoid flammability and related concerns. Sodium nitrate solution is used as the simulant for brine because it is not corrosive and it can match the density ratio between brine and crude oil. The oil is injected downward through a tube into the brine at a prescribed depth below the oil-brine interface. Flow rates are determined by scaling to match the ratio of buoyancy to momentum between the experiment and the SPR. Initially, the momentum of the flow produces a downward jet of oil below the tube end. Subsequently, the oil breaks up into droplets due to shear forces, buoyancy dominates the flow, and a plume of oil droplets rises to the interface. The interface is deflected upward by the impinging oil-brine plume.

Two different diameter injection tubes were used (½-inch and 1-inch OD) to vary the scaling. Use of the 1-inch injection tube also assured that turbulent pipe flow was achieved, which was questionable for lower flow rates in the ½-inch tube. In addition, a ½-inch J-tube was used to direct the buoyant jet upwards rather than downwards to determine whether flow redirection could substantially reduce the oil-plume size and the oil-droplet residence time in the brine. Reductions of these quantities would inhibit emulsion formation by limiting the contact between the oil and the brine.

Videos of this flow were recorded for scaled flow rates that bracket the equivalent pumping rates in an SPR cavern. Image-processing analyses were performed to quantify the penetration depth of the oil jet, the width of the jet, and the deflection of the interface. The measured penetration depths are shallow, as predicted by penetration-depth models, in agreement with the assumption that the flow is buoyancy-dominated, rather than momentum-dominated. The turbulent penetration depth model provided a good estimate of the measured values for the 1-inch injection tube but overpredicted the penetration depth for the ½-inch injection tube. Adding a virtual origin term would improve the prediction for the ½-inch tube for low to nominal injection flow rates but could not capture the rollover seen at high injection flow rates.

As expected, the J-tube yielded a much narrower plume because the flow was directed upward, unlike the downward-oriented straight-tube cases where the plume had to reverse direction, leading to a much wider effective plume area. Larger surface deflections were caused by the narrower plume emitted from the J-tube. Although velocity was not measured in these experiments, the video data showed that the J-tube plume was clearly faster than those emitted from the downward-oriented tubes. These results indicate that oil injection tube modifications could inhibit emulsion formation by reducing the amount of contact (both time and area) between the oil and the brine. Future studies will employ crude oil, saturated brine, and interfacial solids (sludge) from actual SPR caverns.

CONTENTS

Page

FIGURES

TABLES

ACKNOWLEDGMENTS

The authors are grateful to Tom Hinkebein, 6118, for suggesting this work and for his thoughtful oversight and discussions. Ray Finley, 6115, and Steve Webb, 6142, also provided valuable technical oversight and input. Thanks also to the internal reviewers for their careful reviews and helpful suggestions.

EXECUTIVE SUMMARY

An experiment has been performed to investigate oil injection into brine for the Strategic Petroleum Reserve (SPR). The goal is to investigate a new approach to oil reintroduction in SPR. Oil in an SPR cavern must be periodically brought to the surface for degassing. The present approach for returning the degassed oil to the cavern involves cutting off a substantial length of the brine pipe so that it terminates well above the oil-brine interface, pumping the degassed oil back through this shortened pipe so that it reenters the oil-filled region of the cavern, removing the shortened brine pipe, and installing a new full-length brine pipe. Considerable time and expense could be saved if the oil could be injected without modifying the brine pipe. However, this new approach involves injecting the oil below the oil-brine interface and allowing the oil to float up through the brine. One concern involves the degree of emulsification that occurs during this process, including the thickness and properties of the oil-brine layer that forms at the boundary between the oil and brine regions. A critical issue of the proposed process is whether the oil and brine form a stable emulsion at the oil-brine interface after the oil droplets rise through the more dense brine and reach the interface. The experiment is a scale-model flow system (1:10 and 1:20 scale) that maintains the same ratio of buoyancy to momentum as in SPR caverns. The experiment uses silicon oil (Dow Corning 200® Fluid, 5 cSt) and a sodium nitrate solution to simulate the crude oil and brine (saturated sodium chloride solution) in SPR caverns. Image-processing techniques are applied to quantify the penetration depth of the oil jet, the width of the buoyant plume, and the interface deflection. In the future, experiments will be performed using crude oil and brine from SPR caverns.

To support the development of these experiments, an analysis is performed to determine the scaling behavior of the flow. This flow is driven by the downward injection of a buoyant liquid (oil) into an immiscible liquid (brine). The following observations result from this analysis. The oil jet penetrates only a few pipe diameters downward (i.e., a very small distance with respect to cavern length scales) before buoyant forces overwhelm the jet momentum and turn the flow upward. Far from the injection point, the oil volumetric fraction becomes small, indicating that the flow field can be described approximately as a zero-momentum buoyant plume of a single liquid, with oil concentration analogous to temperature. Under this assumption, oil injection 50 feet below the brine layer produces a buoyant plume with a 10-foot diameter at the oil-brine interface, within which the maximum (centerline) oil volume fraction is about 0.03 (3%). Based on the turbulent shear stress of a buoyant plume, oil droplets with diameters in the millimeter range are expected close to the oil-brine interface.

Two classes of experiments are suggested by the analysis. First, a laboratory-scale injection of oil into brine can be examined to verify the buoyant-plume model. This report documents the results of such experiments using simulant fluids. Two different diameter injection tubes were used (½-inch and 1-inch OD) to vary the scaling. In addition, a ½-inch J-tube was used to direct the buoyant jet upwards rather than downwards, to see whether flow redirection could substantially reduce the oil-plume size and the oil-droplet residence time in the brine. Reductions of these quantities would inhibit emulsion formation by limiting the contact between the oil and the brine. Laboratory-scale experiments with SPR crude oil and brine will be performed in the future. Second, oil droplets of prescribed sizes can be injected into brine below the interface, and the oil-brine emulsion layer that results can be monitored as it develops.

The measured penetration depths are shallow, as predicted by the penetration-depth models, in agreement with the assumption that the flow is buoyancy-dominated, rather than momentum-

dominated. The turbulent penetration depth model provided a good estimate of the measured values for the 1-inch injection tube but overpredicted the penetration depth for the ½-inch injection tube. Adding a virtual origin term improves the prediction for the ½-inch tube for low to nominal injection flow rates but could not capture the rollover seen at high injection flow rates.

As expected, the J-tube yielded a much narrower plume because the flow was directed upward, unlike the downward-oriented straight-tube cases where the plume had to reverse direction, leading to a much wider effective plume area. Larger surface deflections were caused by the narrower plume emitted from the J-tube. Although velocity was not measured in these experiments, the video data showed that the J-tube plume was clearly faster than those emitted from the downward-oriented tubes. These results indicate that oil injection tube modifications could inhibit emulsion formation by limiting the contact between the oil and the brine.

INTRODUCTION

The oil stored in the caverns of the Strategic Petroleum Reserve (SPR) absorbs gas from the surrounding formation and must be degassed at regular intervals. Degassing the oil from a cavern is carried out over several months: oil to be degassed is continually withdrawn from the cavern while degassed oil is concurrently reintroduced into the cavern until all the oil has been degassed. Two pipes connecting the surface to the cavern are available for exchange of liquids (see Figure 1). One pipe connects the surface to the top of the cavern and terminates in the oil-filled region. This pipe is used to add or withdraw oil under ordinary operation. The other pipe connects the surface to the bottom of the cavern and terminates in the brine-filled region. This pipe is used to add or withdraw brine under ordinary operation. In the current approach to degassing (as opposed to ordinary operation), the lower portion of the brine pipe is cut off so that the remaining section terminates in the oil-filled region. Oil to be degassed is then withdrawn via the oil pipe, and degassed oil is reintroduced via the shortened brine pipe above the oil-brine interface. After the degassing operation for a cavern is completed, the shortened brine pipe is completely removed, and a new brine pipe equal in length to the original brine pipe is installed.

Considerable time and expense could be saved if the degassed oil could be reintroduced without shortening the brine pipe so that it terminates in the oil-filled region as is currently done (see Figure 1). However, in this new approach, oil would be introduced into the brine-filled region (i.e., below the oil-brine interface). Of particular concern in this new approach is the possible production of an oil-brine emulsion layer at the oil-brine interface. The size and properties of such a layer could adversely affect the storage and future use of the oil. Thus, to assess whether or not the new approach to degassing the oil is feasible, it is necessary to understand the production and properties of an oil-brine emulsion layer formed under such circumstances. Two processes affect the growth and properties of the oil-brine emulsion layer: the flow that produces and transports the oil droplets, and the interaction between these oil droplets and the oil-brine interface.

An experimental investigation is performed to determine the properties, behavior, and growth of the emulsified oil-brine layer between the oil and brine regions. Two classes of experiments are indicated (O'Hern and Torczynski, 2000). First, a downward injection of a buoyant liquid (oil) into an immiscible liquid (brine) can be examined to determine the overall properties of the buoyancy-driven flow that creates and transports droplets to the interface. Second, droplets of the buoyant liquid with prescribed diameters can be injected into the immiscible liquid below the interface, and the resulting layer can be monitored and sampled as it develops. Simulant liquids (e.g., silicon oil and salt water) are used in the initial experiments; however, the actual SPR liquids (crude oil and brine) are ultimately required so that all chemical and physical processes are accurately represented. Scaling analyses developed and reported for these two types of experiments (Torczynski and O'Hern, 2001) are included in this report. These analyses indicate how to scale the oil-brine injection hydrodynamics from an SPR cavern to a laboratory experiment: the ratio of buoyancy effects to momentum effects is kept the same.

In the sections that follow, the laboratory-scale oil-brine injection hydrodynamics experiment is described. In brief, flow systems at 1:10 and 1:20 scale are designed, fabricated, and operated using simulant liquids with hydrodynamic properties similar to oil and brine. Image-processing techniques are applied to determine the plume penetration depth, the plume width, and the interface deflection.

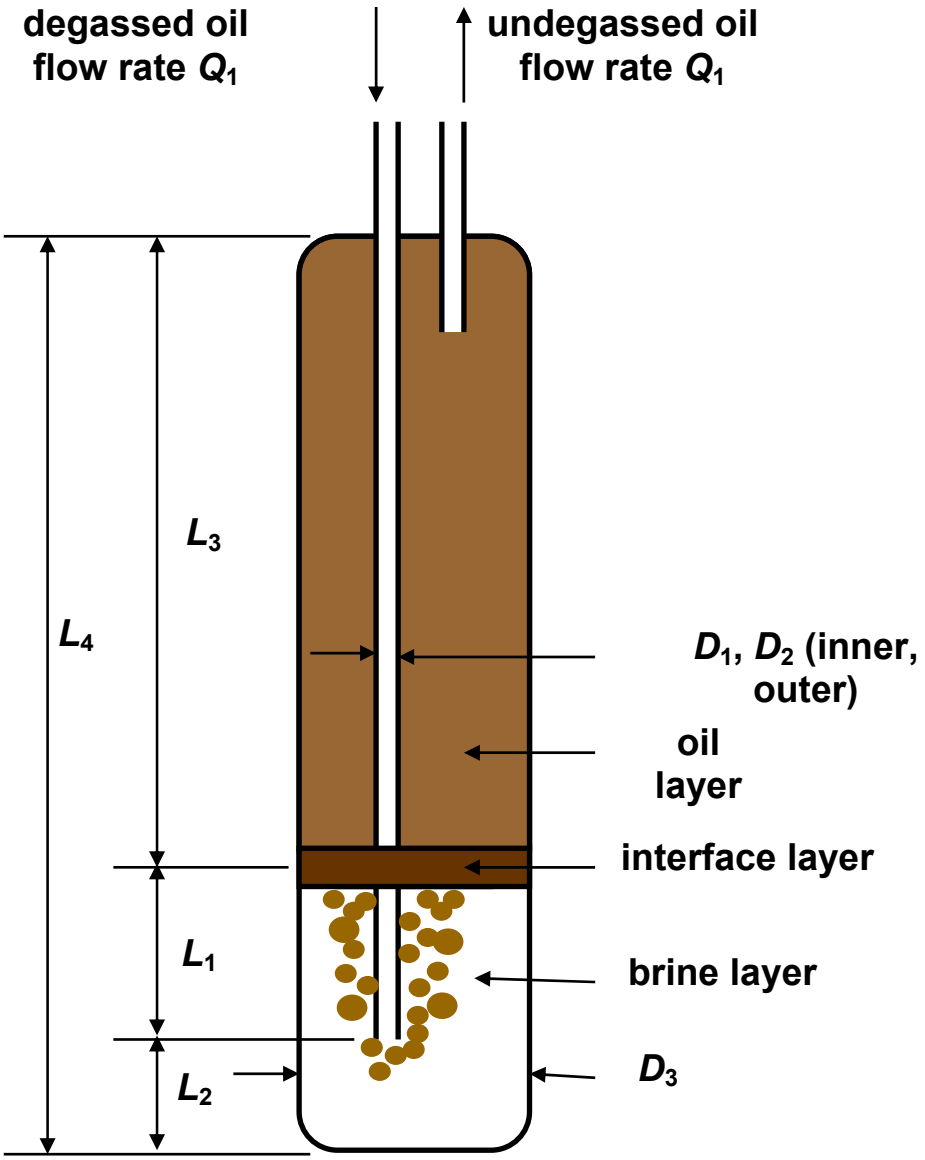

Figure 1. Schematic diagram of the proposed approach for oil reintroduction into an SPR cavern. The diagram is not to scale: in particular, vertical heights are greatly reduced.

SCALING

OIL-INJECTION FLOW

The flow produced by injecting a buoyant liquid (oil) downward into an immiscible liquid (brine) breaks up the oil into droplets and transports them to the oil-brine interface. In the "near field" within several diameters of the pipe end, the oil flows downward into the brine until buoyancy forces overwhelm its momentum. The oil then begins to float upward toward the oil-brine interface. Because of the large length and velocity scales in the system (see Figure 1 and Table 1), the flow is expected to be turbulent. As a result, the turbulent stresses are expected to break apart the oil into smaller and smaller droplets until a size limit is reached below which the interfacial tension between oil and brine prevents further reductions in droplet size. The turbulence also acts to disperse the oil droplets throughout the brine, decreasing the volumetric concentration of the oil while increasing the lateral extent of the droplet-laden brine as the oil floats upward. The buoyant flow produced by the dispersed oil droplets has a large amount of brine entrained as well. It is this large-scale upward flow, rather than the terminal-velocity motion of oil droplets within brine, that is primarily responsible for transporting oil from the pipe end to the oil-brine interface.

After being produced, dispersed, and transported to the oil-brine interface, the oil droplets interact with any materials present at this layer (e.g., an emulsion or sludge). These interactions depend on the size and concentration of the droplets, on the flow properties beneath the layer, and on the physical/chemical properties of the materials.

The proposed oil-reintroduction approach can be described as the downward injection of a buoyant liquid into an immiscible liquid. Depending on the flow parameters, at least two flow patterns could potentially be produced (see Figure 2). The first flow pattern is momentum-dominated, or jet-like: the downward jet reaches the bottom of the cavern, spreads laterally outward, and rises upward at the outer cavern wall. The second flow pattern is buoyancy-dominated, or plume-like: the downward plume penetrates only a fraction of the cavern depth, reverses direction because of buoyancy, rises upward along the injection pipe, and broadens as it rises. Note that the cavern-scale circulations (eddies) produced in these two situations are of opposite sense.

As discussed below, the buoyancy-dominated flow pattern is expected. Based on this, the flow is modeled as a turbulent buoyant plume from a small source (the pipe diameter is much less than cavern length scales, as in Table 1), in which the concentration of oil (present as small, dispersed droplets) is analogous to temperature for a single-phase flow. This model is based on the Boussinesq approximation (Turner, 1979), in which buoyancy is considered to be the only important effect of density differences, and thus is appropriate for describing only the "far-field" flow (i.e., many pipe diameters away from the pipe end). For this approximation to be valid, the oil droplets must be small compared to flow length scales, they must remain dispersed in the brine rather than forming a connected flow path to the interface, and their terminal velocities must be small compared with buoyancy-induced velocities so that turbulent flow and mixing are the dominant transport processes. These constraints appear to be satisfied, as discussed below.

Table 1. Scaling from SPR caverns to laboratory experiment using the same liquids and Froude number (1:10 and 1:20 scales).

Quantity	Symbol/Scaling	Cavern Value	Expt. Value (1:10)	Expt. Value (1:20)
Pipe inner diameter	D_1	0.254 m (10 in)	0.0246 m (0.968 in)	0.012 m (0.468 in)
Pipe length below interface	$L_1 \propto D_1$	15 m (50 ft)	1.2 m (4 ft)	0.60 m (2 ft)
Oil volumetric flow rate (nominal)	$Q_1 \propto D_1^{5/2}$	0.23 m^3/s (range 0.037-0.23 m^3/s)	0.00073 m^3/s	0.00013 m^3/s
Oil average velocity at pipe exit (nominal)	$U_1 \propto D_1^{1/2}$	4.54 m/s (range (0.73-4.54 m/s)	1.44 m/s	1.02 m/s
Buoyancy flow rate	$F_1 \propto D_1^{5/2}$	0.658 m^4/s^3	0.00208 m^4/s^3	0.000368 m^4/s^3
Penetration depth (turbulent)	$z_m \propto D_1$	2.4 m (7.7 ft)	0.24 m (0.77 ft)	0.12 m (0.39 ft)
Penetration depth (frictionless)	$h_m \propto D_1$	3.6 m (12 ft)	0.36 m (1.2 ft)	0.18 m (0.59 ft)
Plume diameter	$2R(L_1) \propto D_1$	3.1 m (10 ft)	0.31 m (1.0 ft)	0.16 m (0.5 ft)
Total volumetric flow rate (entrainment)	$Q(L_1) \propto D_1^{5/2}$	12.5 m^3/s	0.0400 m^3/s	0.0071 m^3/s
Vertical velocity component	$w(0,L_1) \propto D_1^{1/2}$	1.65 m/s	0.52 m/s	0.37 m/s
Turbulent diffusivity	$D_T(0,L_1) \propto D_1^{3/2}$	0.15 m^2/s	0.0047 m^2/s	0.0017 m^2/s
Oil volume fraction	$\varepsilon_o(0,L_1) \propto D_1^{0}$	0.03	0.03	0.03
Reynolds number	$Re \propto D_1^{3/2}$	920,000	29,000	10,000
Maximum isolated droplet diameter	$d_{max} \propto D_1^{0}$	15 mm	15 mm	15 mm
Pipe wall thickness	$(D_2 - D_1) \propto D_1^{1}$	9.5 mm (3/8 in)	0.95 mm (0.038 in)	0.48 mm (0.019 in)
Cavern diameter (vessel width)	$D_3 >> L_1$	61 m (200 ft)	0.9 m (3 ft)	0.9 m (3 ft)
Pipe exit height above bottom	$L_2 >> \max(z_m,h_m)$	92 m (300 ft)	0.76 m (2.5 ft)	1.37 m (4.5 ft)
Interface depth below top	L_3	503 m (1650 ft)	0.45 m (1.5 ft)	0.45 m (1.5 ft)

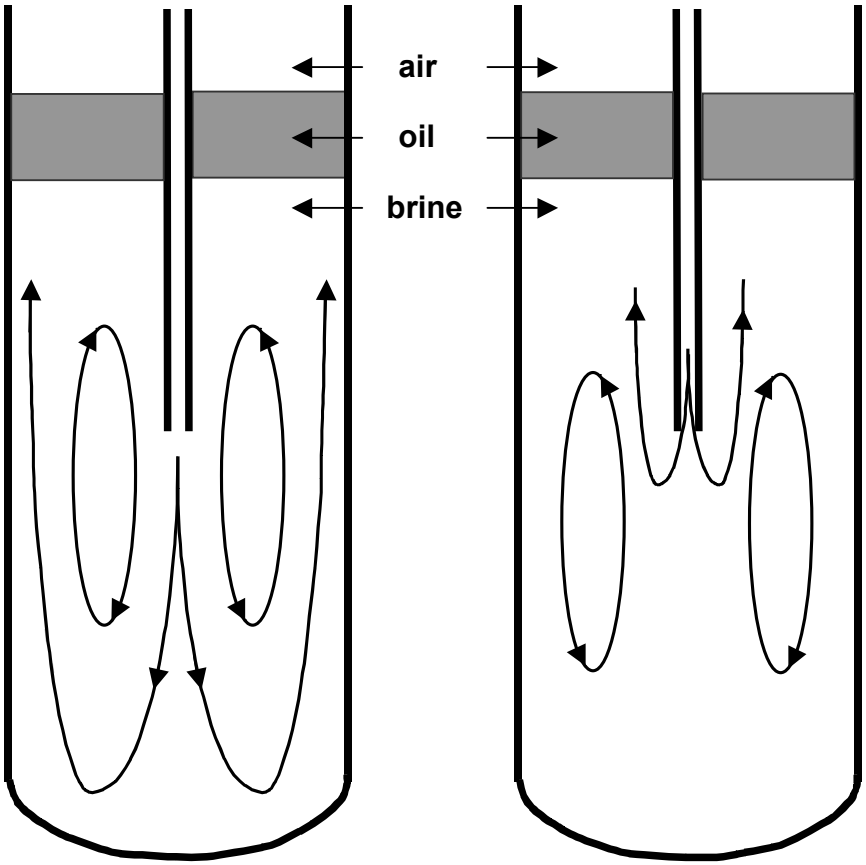

Figure 2. Two possible flow patterns: left, momentum-dominated; right, buoyancy-dominated. The buoyancy-dominated regime is expected in SPR caverns.

Penetration Depth Model

To determine whether the flow is initially momentum-dominated or buoyancy-dominated in typical cavern conditions, the penetration depth of the downward oil plume is estimated. If the penetration depth is found to be much smaller than the distance from the pipe end to the cavern bottom, then the buoyancy-dominated flow regime is obtained. Turner (1979) provides a similarity-solution estimate of the penetration depth z_m for a downward-directed turbulent jet of buoyant liquid into a miscible liquid:

$$\frac{z_m}{D_1} = 1.85\left(\frac{\pi}{4}\right)^{\frac{1}{4}}\left[\frac{\rho_b U_1^2}{(\rho_b - \rho_o)gD_1}\right]^{\frac{1}{2}},\ U_1 = \frac{Q_1}{(\pi/4)D_1^2}, \tag{1}$$

or, defining the Froude number $Fr = \dfrac{\rho_b U_1^2}{(\rho_b - \rho_o)gD_1}$, Equation (1) becomes

$$\frac{z_m}{D_1} = 1.85\left(\frac{\pi}{4}\right)^{\frac{1}{4}} Fr^{\frac{1}{2}} \tag{2}$$

where ρ_b and ρ_o are the mass densities of the brine and oil, respectively, g is the gravitational acceleration, Q_1 is the volumetric flow rate of the oil, D_1 is the inner diameter of the pipe, and U_1 is the oil average velocity exiting the pipe end (0.73 and 4.54 m/s for the minimum and maximum flow rates for a cavern, as in Table 1). For the minimum and maximum flow rates and other parameters in Tables 1 and 2, this model predicts a penetration depth between 0.4 and 2.4 m (between 1.5 and 9 diameters). These values are much smaller than the height of the pipe end above the cavern bottom (nominally 92 m) and the height of the interface above the pipe end (at least 15 m, possibly up to 426 m). An upper bound for the penetration depth is obtained by considering the depth h_m reached by an object with the same density as oil if injected downward into brine with a velocity equal to that of the oil exiting the pipe, where drag is conservatively neglected (frictionless flow):

$$\frac{h_m}{D_1} = \left(\frac{1}{2}\right)\left[\frac{\rho_b U_1^2}{(\rho_b - \rho_o) g D_1}\right] = \frac{1}{2} Fr. \tag{3}$$

This upper bound results from assuming that the object experiences only gravitational and buoyancy forces, which are constant. For the parameter values in Table 1 and the minimum and maximum oil flow rates, the depth h_m has values of 0.1 and 3.6 m (0.4 and 14 diameters), respectively. Thus, for both estimates, the oil jet penetrates roughly 1 diameter below the pipe end at the minimum flow rate and 10 diameters below the pipe end for the maximum flow rate, both of which are small compared to cavern length scales. The small penetration-depth values indicate that the momentum of the jet is negligible compared to buoyancy and that the buoyancy-dominated regime is obtained.

Turbulent Buoyant Plume

The small penetration depth determined in the previous section suggests that the flow in the region between the pipe end and the oil-brine interface can be described as a buoyancy-dominated turbulent plume. Turner (1979) presents closed-form approximate results for a buoyant turbulent plume, in which buoyancy is produced by the nonuniform distribution of temperature. These expressions can be used to describe the oil-brine plume in the far field (i.e., many diameters from the pipe end) so long as the following constraints hold. The oil droplets must be small compared to the plume length scales, they must be dispersed and not form a connected flow path through the brine from the pipe end to the interface, and they must have small terminal velocities compared with buoyancy-induced velocities so that turbulent flow and mixing are the dominant transport processes. Under these restrictions, the following similarity results are obtained (Turner, 1979):

$$F_1 = \left(\frac{\rho_b - \rho_o}{\rho_b}\right) g Q_1 \text{ (buoyancy flow rate)}, \tag{4}$$

$$\pi ac = b + d \quad \text{(flow rate consistent with } Q_1\text{)}, \tag{5}$$

$$Q(z) = (\pi a/b)(F_1 z^5)^{1/3} \quad \text{(total volumetric flow rate)}, \tag{6}$$

$$R(z) = z/b^{1/2} \quad (1/e \text{ radius of vertical velocity component}), \tag{7}$$

$$\frac{g[\rho_b - \rho(r,z)]}{\rho_b} = c\left(\frac{F_1^2}{z^5}\right)^{\frac{1}{3}} \exp\left[-d\left(\frac{r}{z}\right)^2\right] \quad \text{(buoyancy)}, \tag{8}$$

$$\varepsilon_o(r,z) = \frac{\rho_b - \rho(r,z)}{\rho_b - \rho_o} \text{ or } \rho(r,z) = \rho_b[1-\varepsilon_o(r,z)] + \rho_o\varepsilon_o(r,z) \quad \text{(oil volume fraction)}, \tag{9}$$

$$w(r,z) = a\left(\frac{F_1}{z}\right)^{\frac{1}{3}} \exp\left[-b\left(\frac{r}{z}\right)^2\right] \quad \text{(vertical velocity component)}, \tag{10}$$

$$u(r,z) = \frac{\left(\frac{F_1}{z}\right)^{\frac{1}{3}}\left\{ar^2 \exp\left[-b\left(\frac{r}{z}\right)^2\right] - \left(\frac{5a}{6b}\right)z^2\left(1-\exp\left[-b\left(\frac{r}{z}\right)^2\right]\right)\right\}}{rz}$$

(radial velocity component), (11)

$$D_T(r,z) = (F_1 z^2)^{\frac{1}{3}}\left\{\frac{5a\left(1-\exp\left[-b\left(\frac{r}{z}\right)^2\right]\right)}{2b\left(\frac{r}{z}\right)^2\left[6d\left(1+\left(\frac{r}{z}\right)^2\right)-5\right]}\right\} \quad \text{(turbulent diffusivity)}, \tag{12}$$

$$a = 4.7,\ b = 96,\ d = 71, \text{ so } c = 167/(4.7\pi) \approx 11.31 \quad \text{(preferred parameter values)}. \tag{13}$$

These relations describe a turbulent buoyant single-phase plume that arises from a point source of buoyancy of strength F_1 (proportional to the volumetric flow rate Q_1). Here, the buoyancy source is located at a distance comparable to the penetration depth below the pipe end. Because of the smallness of the penetration depth (shown in the previous section) relative to the distance from the pipe end to the oil-brine interface, the plume origin (z = 0) is taken to be coincident with the pipe end. Note that the volumetric flow rate in the plume increases with height. This is because the rising turbulent plume mixes with and entrains the surrounding brine. Because the plume is self-similar, the plume width R is proportional to the height z above its origin and does not depend on the strength of the buoyancy source. Additionally, as the height above the origin is

increased, the velocity components and the oil volume fraction decrease, but the turbulent diffusivity increases.

Table 3 shows values for some of the plume quantities that are determined using the parameter values in Tables 1 and 2. These quantities are evaluated along the centerline of the plume ($r = 0$) near the oil-brine interface ($z = L_1$) for the minimum and maximum flow rates ($Q_1 = 0.037$ m^3/s and $Q_1 = 0.23$ m^3/s, respectively). Independent of flow rate, the plume grows to a diameter of about 3.1 m (10 feet) near the oil-brine interface. The total volumetric flow present in the plume is 185 times the oil flow rate for the minimum-flow situation and 54 times the oil flow rate for the maximum-flow situation. Thus, a large volume of brine is entrained by the upward flow of oil. Flow speeds around 0.9-1.7 m/s and turbulent diffusivities of 0.08-0.15 m^2/s are produced near the oil-brine interface. From Table 2, these turbulent-diffusivity values are seen to be larger than the kinematic viscosities of oil or brine by a factor of 10^5. The oil volume fraction is seen to lie in the range of 0.01-0.03, which is consistent with the assumption of dispersed droplet flow. Near the pipe exit (say, $z \le L_1/10$), the expression for oil volume fraction indicates values around unity. Correspondingly, the plume diameter at this height becomes comparable to the pipe diameter. These facts indicate that the model is not valid close to the pipe end, as indicated earlier. Nevertheless, the model indicates oil volume fractions of at most a few percent, flow velocities in the range of 1-2 m/s, and turbulent diffusivities around 0.1 m^2/s near the oil-brine interface.

Table 2. Parameters and nominal values for SPR oil reintroduction into brine. Bracketed values indicate extreme conditions.

Parameter	Symbol	Nominal Value
Pipe inner diameter	D_1	0.254 m (10 inch)
Pipe outer diameter	D_2	0.273 m (10 3/4 inch)
Cavern diameter	D_3	61 m (200 feet)
Pipe length below interface	L_1	15 m (50 feet) [426 m (1400 feet)]
Pipe height above cavern bottom	L_2	92 m (300 feet)
Interface depth below cavern top	L_3	503 m (1650 feet) [92 m (300 feet)]
Cavern bottom-to-top height	L_4	610 m (2000 feet), $L_1 + L_2 + L_3$
Oil volumetric flow rate	Q_1	0.037-0.230 m^3/s ((20-125)·10^3 bbl/day)
Gravitational acceleration	g	9.81 m/s^2
Temperature	T	313 K (40 °C)
Oil mass density	ρ_o	850 kg/m^3
Oil viscosity	μ_o	0.0040 kg/(m·s) ±50%
Oil kinematic viscosity	$\nu_o = \mu_o/\rho_o$	4.7×10^{-6} m^2/s ±50%
Saturated brine mass density	ρ_b	1200 kg/m^3
Saturated brine viscosity	μ_b	0.0015 kg/(m·s)
Saturated brine kinematic viscosity	$\nu_b = \mu_b/\rho_b$	1.25×10^{-6} m^2/s ±50%
Interfacial (surface) tension	σ	0.05 J/m^2 ±60%

Table 3. Plume characteristics on centerline ($r = 0$) near the oil-brine interface ($z = L_1$).

Quantity	Symbol	At Minimum Flow	At Maximum Flow
Pipe length below interface	L_1	15 m	15 m
Plume diameter	$2R(L_1)$	3.1 m = 12 D_1	3.1 m = 12 D_1
Buoyancy flow rate	F_1	0.105 m^4/s^3	0.658 m^4/s^3
Total volumetric flow rate	$Q(L_1)$	6.8 m^3/s = 185 Q_1	12.5 m^3/s = 54 Q_1
Vertical velocity component	$w(0,L_1)$	0.9 m/s	1.7 m/s
Turbulent diffusivity	$D_T(0,L_1)$	0.08 m^2/s	0.15 m^2/s
Oil volume fraction	$\varepsilon_o(0,L_1)$	0.01	0.03

Droplet Terminal Velocity

In selecting the turbulent buoyant plume model of the previous section, it is assumed that the velocities of the oil droplets relative to the brine are small with respect to the flow velocities of the plume itself. Clift, Grace, and Weber (1978) provide a correlation in graphical form (see Figure 3) for estimating the terminal velocity U of an isolated droplet of effective diameter d_e (the diameter of the sphere having the same volume as the droplet) in terms of the Eotvos, Morton, and Reynolds numbers and the density and viscosity ratios:

$$Eo = g(\rho_b - \rho_o)d_e^2/\sigma \text{ (Eotvos number)}, \tag{14}$$

$$Mo = g\mu_b^4(\rho_b - \rho_o)/\rho_b^2\sigma^3 \text{ (Morton number)}, \tag{15}$$

$$Re = \rho_b U d_e/\mu_b \text{ (Reynolds number)}, \tag{16}$$

$$\gamma = \rho_o/\rho_b \text{ (density ratio)}, \tag{17}$$

$$\kappa = \mu_o/\mu_b \text{ (viscosity ratio)}. \tag{18}$$

Table 4 shows values of these parameters and the corresponding terminal velocities for three droplet diameters. It is later shown that these diameters probably bound the droplet sizes that actually exist in the plume flow. In all cases, the terminal velocities are much less than the flow speeds that exist in the plume. Moreover, terminal velocities are typically reduced when droplets are not isolated (Davis and Acrivos, 1985). These facts indicate that the assumption of a small relative velocity between the oil and brine with respect to the flow velocity is probably valid.

Table 4. Terminal velocities of isolated droplets of oil in brine.

Quantity	Symbol	d_e = 0.1 mm	d_e = 1 mm	d_e = 10 mm
Density ratio	γ	0.708	0.708	0.708
Viscosity ratio	κ	2.67	2.67	2.67
Morton number	Mo	9.66×10^{-11}	9.66×10^{-11}	9.66×10^{-11}
Eotvos number	Eo	6.87×10^{-4}	6.87×10^{-2}	6.87×10^{0}
Reynolds number	Re	0.10	50	1200
Terminal velocity	U	0.0013 m/s	0.063 m/s	0.15 m/s
Droplet type	n/a	spherical	deformed	wobbling

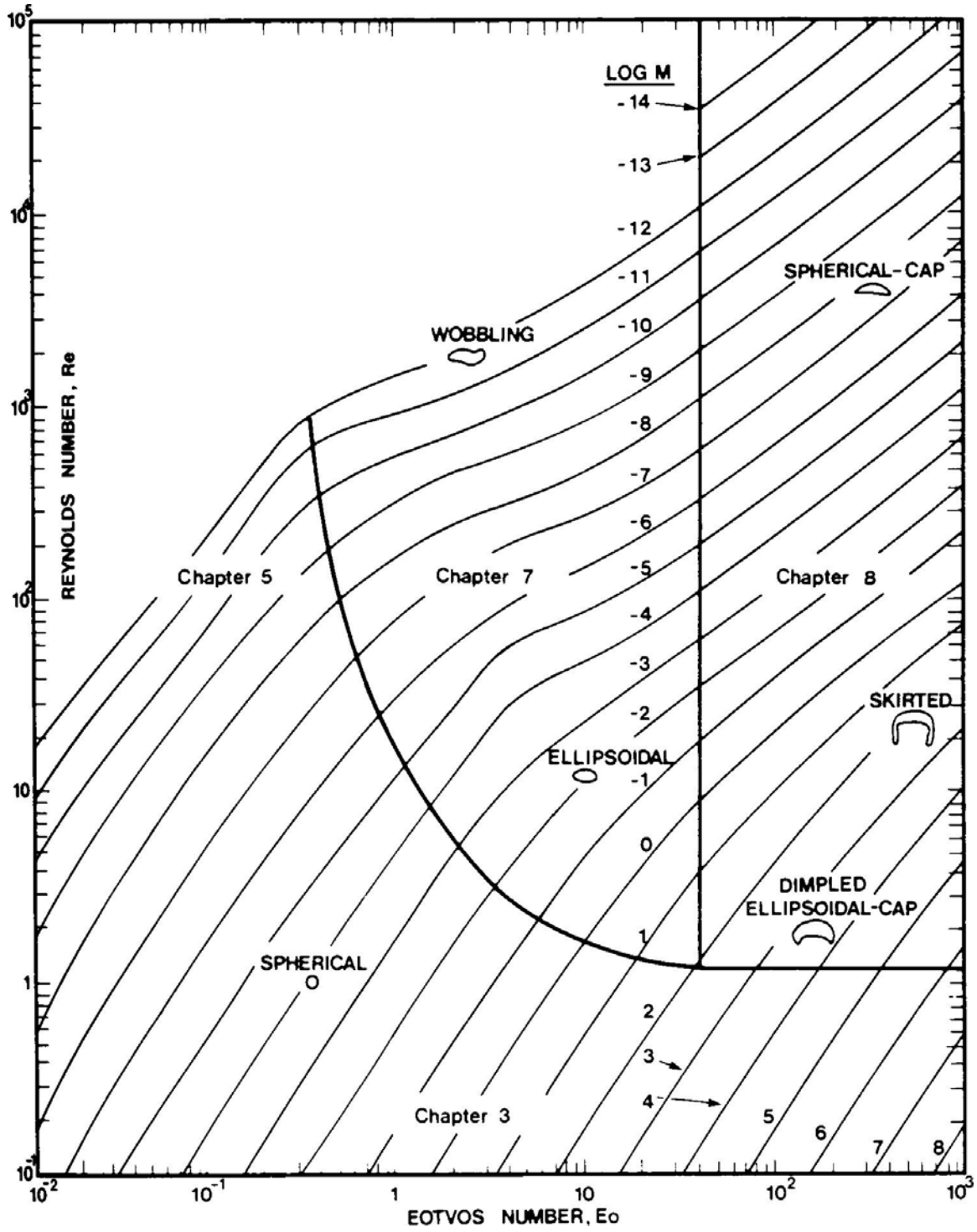

Figure 3. Graphical correlation of isolated droplet terminal velocity in terms of Eotvos, Morton, and Reynolds numbers (Clift, Grace, and Weber, 1978).

OIL-DROPLET SIZE DISTRIBUTION

To understand the formation, growth, and properties of an emulsified layer between the oil and brine regions, it is necessary to determine the size distribution of the oil droplets in the plume beneath the interface. Estimates of the maximum and minimum droplet sizes are presented below, with the most probable size located somewhere between.

Clift, Grace, and Weber (1978) present an estimate of the maximum stable effective diameter d_{max} for an isolated droplet rising at its terminal velocity (droplets with $d_e \geq d_{max}$ are unstable because of the Rayleigh-Taylor instability):

$$d_{max} = 4\left(\frac{\sigma}{g(\rho_b - \rho_o)}\right)^{\frac{1}{2}}. \tag{19}$$

Using the values in Table 1, the maximum stable effective diameter is seen to be $d_{max} = 15$ mm. Flow nonuniformities, as expected in the buoyant plume, can significantly decrease this value: velocity gradients rotate and deform the droplets, and interfacial tension may be too small to prevent break up.

Clift, Grace, and Weber (1978) also provide an estimate of the minimum unstable effective diameter d_{min} for an isolated droplet in a turbulent flow field (droplets with $d_e \leq d_{min}$ are stable):

$$d_{min} = \frac{\sigma + \mu_o\sqrt{\tau/\rho_o}}{\tau} \approx \frac{\sigma}{\tau}, \tag{20}$$

where τ is the local shear stress (the second addend in the numerator is small for the parameter values considered here). An approximate upper bound for the shear stress near the oil-brine interface can be taken from the buoyant plume model described in the previous sections:

$$\tau \sim \frac{\rho_b D_T(0, L_1) w(0, L_1)}{R(L_1)}. \tag{21}$$

Using the parameter values in Tables 1-2, minimum unstable effective diameters of $d_{min} = 0.9$ mm and $d_{min} = 0.3$ mm are found for the minimum and maximum oil volumetric flow rates, respectively. The uncertainty associated with these values is substantial for several reasons. First, the above expression probably overestimates the shear stress that is available on the droplet scale to induce breakup. A smaller τ value would increase d_{min}. Second, the shear stress is largest near the pipe exit and decreases as the flow moves toward the oil-brine interface. A larger τ value would decrease d_{min}. Third, droplet formation may be strongly affected by the near-field flow as oil is injected downward into the brine, which is not considered in the above description. Fourth, the interfacial tension σ has a substantial uncertainty and can be significantly altered by the presence of surface-active chemical species in trace amounts.

Based on the above results, it is concluded that the oil droplets probably have diameters distributed roughly within the range 0.1 mm < d_e < 10 mm. Note that these values are much less than the pipe diameter $D_1 = 254$ mm. Droplet diameters were not measured in the experiments reported here. However, visual observations support the 0.1-10 mm range predicted here.

PLUME HYDRODYNAMICS EXPERIMENT

A plume hydrodynamics experiment is developed to determine whether the turbulent buoyant flow predicted using miscible-liquid arguments is representative of the actual immiscible two-phase flow that occurs during oil reintroduction into brine in an SPR cavern. To develop a laboratory-scale experiment that accurately represents the cavern-scale flow, it is necessary to perform a scaling analysis of this flow. Based on Figure 1 and Table 1, the flow is controlled by nine parameters, shown in Table 5. Six are physical or thermophysical parameters, one is an operating parameter, and two are geometric parameters. Although there are other geometric parameters, they are either large enough to be considered infinite (e.g., L_2, the distance from the pipe end to the cavern bottom; and D_3, the cavern diameter) or small enough to be considered zero (e.g., $(D_2 - D_1)/2$, the pipe wall thickness). Although there may be additional parameters by virtue of the presence of surface-active chemical species, their cumulative effects are assumed to be represented by the interfacial tension.

Table 5. Parameters that control scaling of oil reintroduction into brine.

Quantity	Symbol	Parameter Type	MKS Units
Gravitational acceleration	g	physical	m/s^2
Brine mass density	ρ_b	thermophysical	kg/m^3
Oil mass density	ρ_o	thermophysical	kg/m^3
Brine absolute viscosity	μ_b	thermophysical	kg/(m·s)
Oil absolute viscosity	μ_o	thermophysical	kg/(m·s)
Oil-brine interfacial (surface) tension	σ	thermophysical	kg/s^2
Oil average velocity at pipe end	U_1	operating	m/s
Pipe inner diameter	D_1	geometric	m
Pipe length below interface	L_1	geometric	m

Because there are nine dimensional parameters and three physical units (length, time, and mass), exactly six nondimensional parameters can be formed for scaling purposes. One such set of nondimensional parameters is suggested below (this set is not unique):

$$\gamma = \frac{\rho_o}{\rho_b} \text{ (density ratio)}, \tag{22}$$

$$\kappa = \frac{\mu_o}{\mu_b} \text{ (viscosity ratio)}, \tag{23}$$

$$A = \frac{L_1}{D_1} \text{ (aspect ratio)}, \tag{24}$$

$$Fr = \frac{\rho_b U_1^2}{(\rho_b - \rho_o) g D_1} \text{ (Froude number)}, \tag{25}$$

$$Re = \frac{\rho_b U_1 D_1}{\mu_b} \text{ (Reynolds number),} \tag{26}$$

$$\frac{1}{Bo} = \frac{\sigma}{(\rho_b - \rho_o) g D_1^2} \text{ (inverse Bond number).} \tag{27}$$

The inverse of the Froude number is called the Richardson number, and the Bond number is often called the Eotvos number when referring to droplets.

In developing a laboratory experiment that reproduces the important features of oil reintroduction into brine, it is necessary to reproduce the values of the above nondimensional parameters. The density and viscosity ratios are easily reproduced by working with the actual liquids (oil and brine); in fact, most immiscible pairs of common liquids yield fairly similar values for these parameters. The aspect ratio is easily reproduced by scaling all lengths proportionally from the actual flow geometry. However, the cavern values of the Froude, Reynolds, and inverse Bond numbers cannot all be reproduced on the laboratory scale. Since most liquids have densities that are within 20% of the value for water and viscosities that are comparable to or exceed the value for water, fixing the Froude number implies that the Reynolds number is greatly reduced, whereas fixing the Reynolds number implies that the Froude number is greatly increased. Because the Froude number gauges the strength of the buoyancy forces that drive the flow (as seen from a detailed examination of Equations 1 through 13), a change in Froude number modifies the buoyancy forces correspondingly. However, since flows with large Reynolds numbers are fairly independent of Reynolds number (at least at plume-diameter length scales although not at the scales of the smallest eddies), even a significant reduction in Reynolds number may not change the overall flow behavior significantly (Turner, 1979). Thus, the Froude number for the laboratory experiment is set equal to that of the cavern flow. The value of the inverse Bond number also cannot be maintained when scaling from the cavern flow to the laboratory experiment. However, the inverse Bond number is seen to be proportional to $(d_{max}/D_1)^2$, where d_{max} is the maximum isolated droplet size, as in Equation 19. If d_{max} sets the scale for the droplet size in the cavern flow and the laboratory experiment, then droplets of about the same size would be produced in both flows despite the increase in the inverse Bond number. This might actually be desirable and allow the interaction of the droplets with the oil-brine layer at the interface to be accurately reproduced in the laboratory experiment.

Table 6 shows a comparison between the cavern flow and the laboratory experiment. The values in this table are determined by setting the laboratory length parameters equal to one-tenth of the corresponding cavern values while preserving the cavern value of the Froude number (and using the same liquid properties). Although the Reynolds number in the experiment is substantially reduced from the cavern value, it is large enough to sustain turbulent flow.

Table 6. Experimental conditions for the three different injection tubes.

Quantity	½-inch tube	1-inch tube	½-inch J-tube
Tube OD	0.500 inch	1.000 inch	0.500 inch
Tube ID	0.468 inch	0.960 inch	0.468 inch
Injection flow rate	0.42-3.1 GPM	1.28-12.8 GPM	0.46-3.1 GPM
Injection velocity	0.24-1.78 m/s	0.39-3.89 m/s	0.26-1.76 m/s
Depth below interface	0.60 m (24 in)	1.2 m (48 in)	0.60 m (24 in)
Oil layer thickness	0.30 m (12 in)	0.30 m (12 in)	0.30 m (12 in)
Brine layer thickness	1.98 m (78 in)	1.98 m (78 in)	1.98 m (78 in)
Air layer thickness	0.15 m (6 in)	0.15 m (6 in)	0.15 m (6 in)

EXPERIMENTAL SETUP AND PROCEDURES

A laboratory-scale oil-brine injection hydrodynamics experiment has been designed and constructed to examine the hydrodynamics of downward injection of oil into brine and the immiscible buoyant plume of droplets that results. The purpose of this experiment is to determine the validity of the scaling analysis. Of particular interest are plume characteristics (penetration depth, width of plume, impact on interface) and the size, velocity, and concentration of the oil droplets in the vicinity of the oil-brine interface. This information is of basic interest and is needed as input to develop the oil-brine interface emulsification experiment.

Vessel and Flow System

Figure 4 shows a photograph of the experimental vessel, and Tables 6 and 7 show parameters for the experiment corresponding to the schematic diagram in Figure 1. The vessel is an acrylic tube that has an inner diameter of 0.889 m (35 inches), a wall thickness of 1.27 cm (0.5 inch), and a height of 2.44 m (96 inches or 8 feet). A square base plate with an inflatable O-ring gasket forms the bottom of the vessel. This base plate is held 0.61 m (2 feet) above the floor by a Unistrut® frame. A penetration through the base plate allows draining of the liquids for storage or disposal. A square metallic top plate covers the upper opening of the vessel. This top plate is tethered by cables from each of its four corners to the corresponding corners of the base plate. These cables are under sufficient tension to prevent the cylinder from "floating", which could otherwise occur because the force from the liquid hydrostatic pressure on the cylinder base edge exceeds the cylinder weight (i.e., the liquid is on average more dense than the material comprising the cylinder).

A continuously operating flow loop is installed in the vessel to drive the oil injection. A Viking H32 pump driven by a ¾-HP Baldor Industrial Motor M3542 is used to pump oil from the oil layer through the injection tube and into the brine layer. The injected oil breaks up into droplets that float up to the oil-brine interface and merge into the oil layer above. The pump intake is a 2.54-cm (1-inch) diameter pipe positioned within the oil layer. The injection tube and the oil intake both pass through the square top plate on the vessel. Three injection tubes are used in these experiments, as shown in Table 6 and Figures 5 through 7: nominal ½-inch-ID and 1-inch-ID straight tubes, and a ½-inch-ID "J-tube". Use of the 1-inch injection tube assured that turbulent pipe flow was achieved, which was questionable for lower flow rates in the ½-inch tube. The end of the ½-inch J-tube has been shaped to direct the oil upward rather than

downward to see whether flow redirection can substantially reduce the oil-plume size and the oil-droplet residence time in the brine. Reductions of these quantities would inhibit emulsion formation by limiting the contact between the oil and the brine. Table 7 shows that the experimental injection velocities bracketed the nominal value corresponding to an SPR injection of 125,000 barrels/day.

Oil flow rates are measured and logged with an ultrasonic flow meter (Controlotron Stormmeter 1010, Uniflow, Universal Portable Flowmeter). This flow meter provides a simple clamp-on flow rate measurement. Figures 8 through 10 show the measured oil flow rates during the three test series. Figure 11 shows the relationship between pump motor RPM and oil volumetric flow rate. This is a useful reference as some of the subsequent data are presented with motor RPM as a parameter. Table 7 summarizes the flow conditions examined and includes their scaled values for use in the SPR. As indicated earlier, the laboratory flow conditions are chosen so that the laboratory value of the Froude number matches the cavern value.

Table 7. Test conditions for oil injection experiments.

Pipe	Motor RPM	Flow Rate (GPM)	Oil Exit Velocity (ft/s)	Oil Exit Velocity (m/s)	Lab Flow Rate Scaled to Cavern Conditions (bbl/day)	Lab Oil Exit Velocity Scaled to Cavern Conditions (m/s)
0.5 in	41	0.424	0.791	0.241	30656	1.11
0.5 in	83	1.014	1.891	0.576	73346	2.66
0.5 in	104	1.300	2.425	0.739	94115	3.42
0.5 in	145	1.848	3.447	1.051	133735	4.86
0.5 in	166	2.147	4.005	1.221	155361	5.64
0.5 in	208	2.817	5.254	1.602	203821	7.40
0.5 in	229	3.128	5.834	1.778	226365	8.22
1.0 in	104	1.282	0.568	0.173	15388	0.56
1.0 in	145	1.850	0.820	0.250	22214	0.81
1.0 in	208	2.850	1.264	0.385	34228	1.24
1.0 in	270	3.604	1.598	0.487	43277	1.57
1.0 in	416	5.274	2.338	0.713	63327	2.30
1.0 in	583	7.361	3.263	0.995	88393	3.21
1.0 in	624	7.875	3.491	1.064	94559	3.43
1.0 in	729	9.234	4.093	1.248	110887	4.03
1.0 in	854	10.727	4.755	1.450	128807	4.68
1.0 in	1020	12.765	5.659	1.725	153286	5.57
0.5 in J	41	0.460	0.858	0.262	33309	1.21
0.5 in J	83	0.996	1.858	0.566	72039	2.62
0.5 in J	104	1.255	2.341	0.713	90794	3.30
0.5 in J	145	1.810	3.376	1.029	130969	4.76
0.5 in J	166	2.130	3.973	1.211	154142	5.60
0.5 in J	208	2.785	5.195	1.583	201495	7.32
0.5 in J	229	3.098	5.778	1.761	224152	8.14

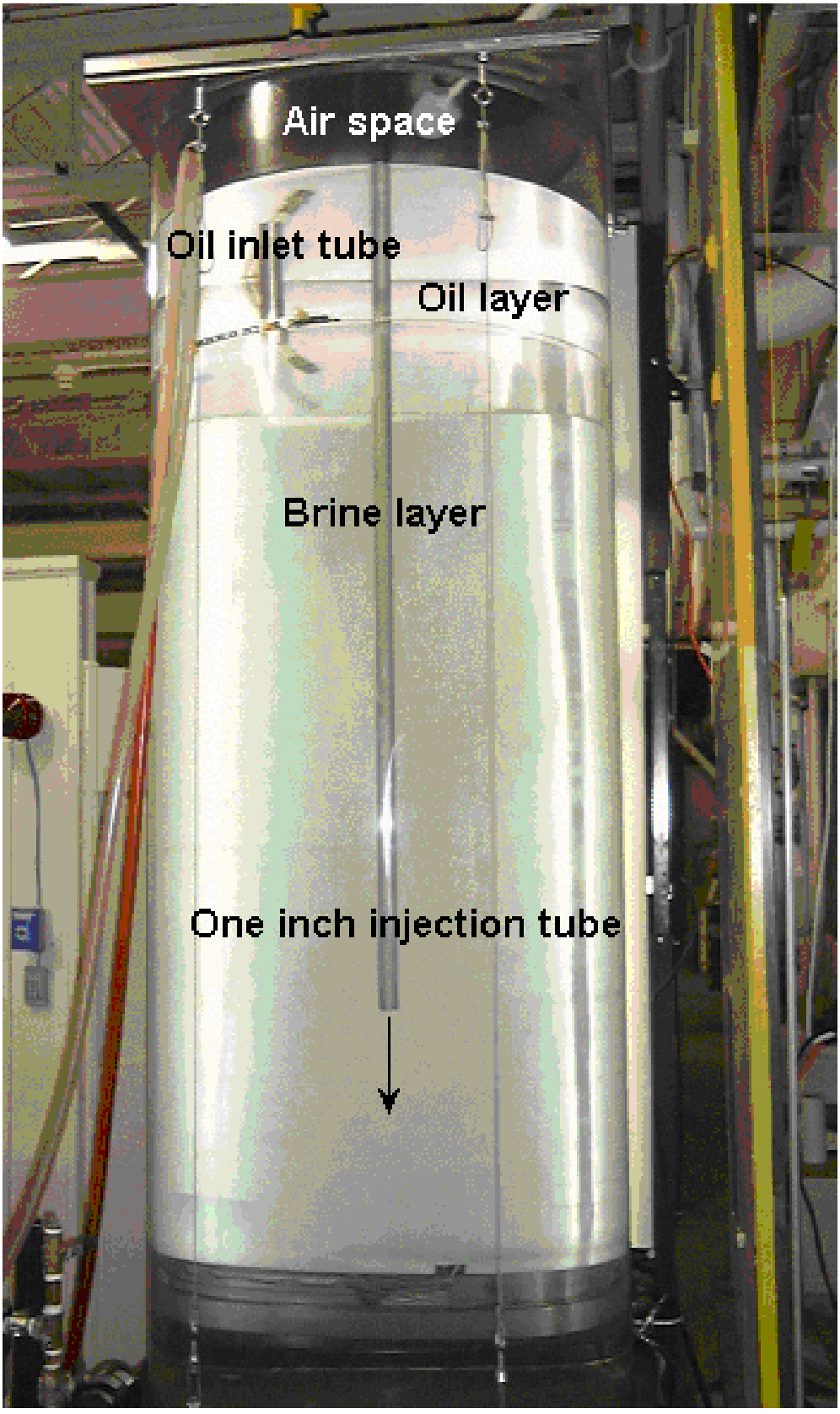

Figure 4. Photograph of the oil-brine injection hydrodynamics experiment for SPR.

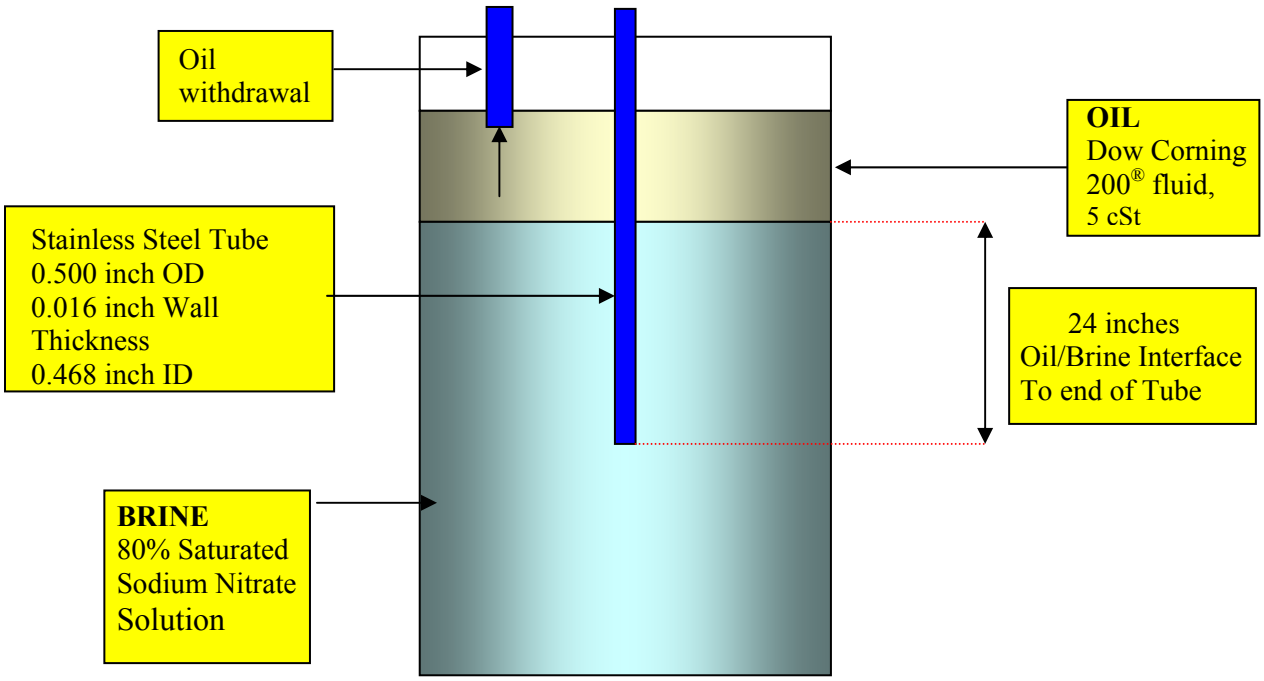

Figure 5. Experimental setup with ½-inch straight tube (1:20 scale).

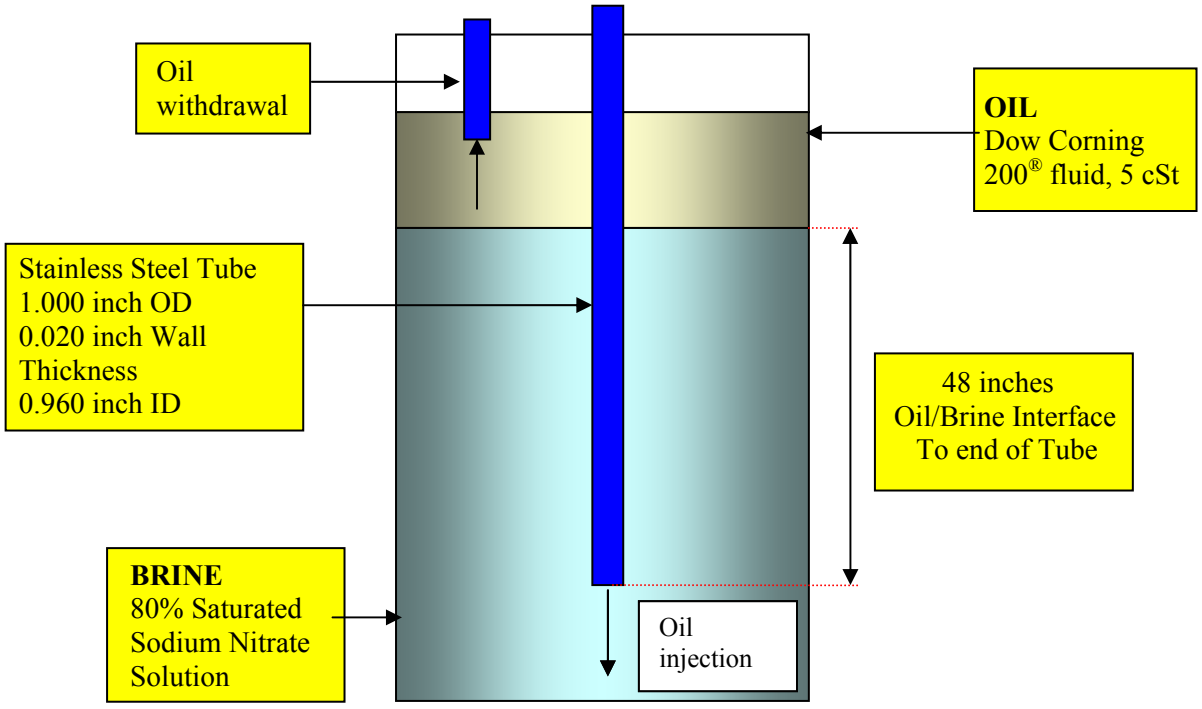

Figure 6. Experimental setup with 1-inch straight tube (1:10 scale).

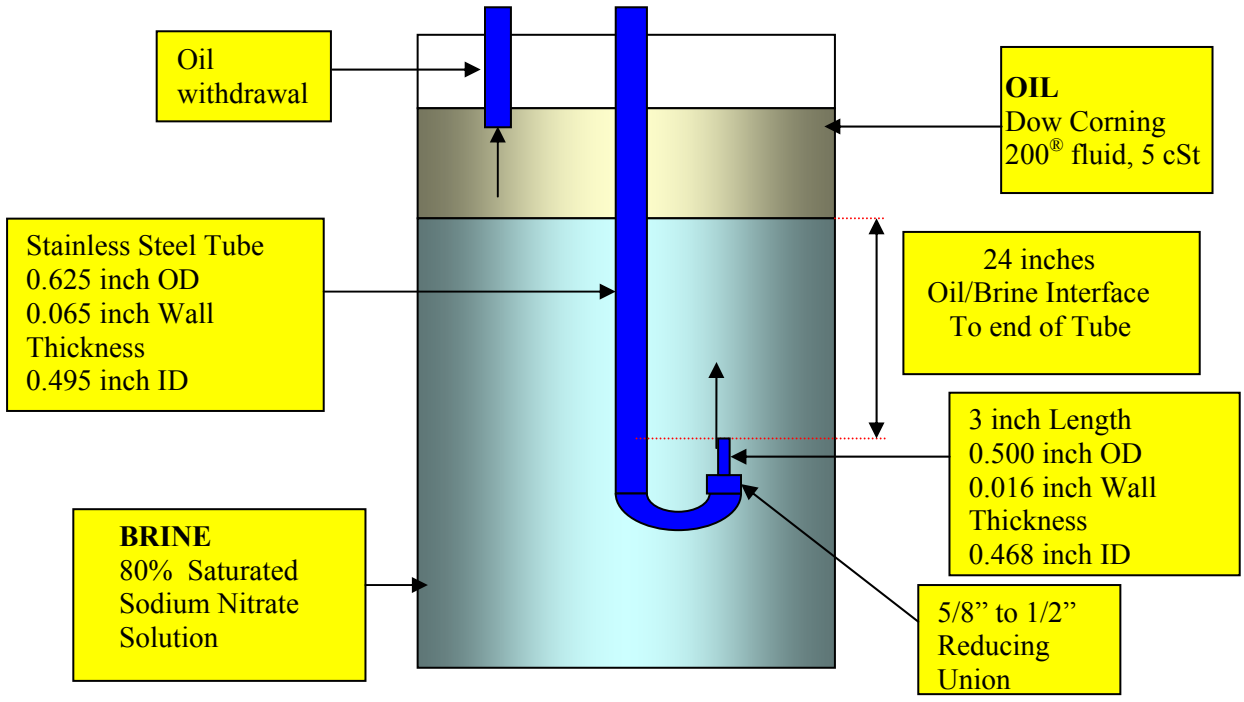

Figure 7. Experimental setup with ½-inch J-tube (1:20 scale).

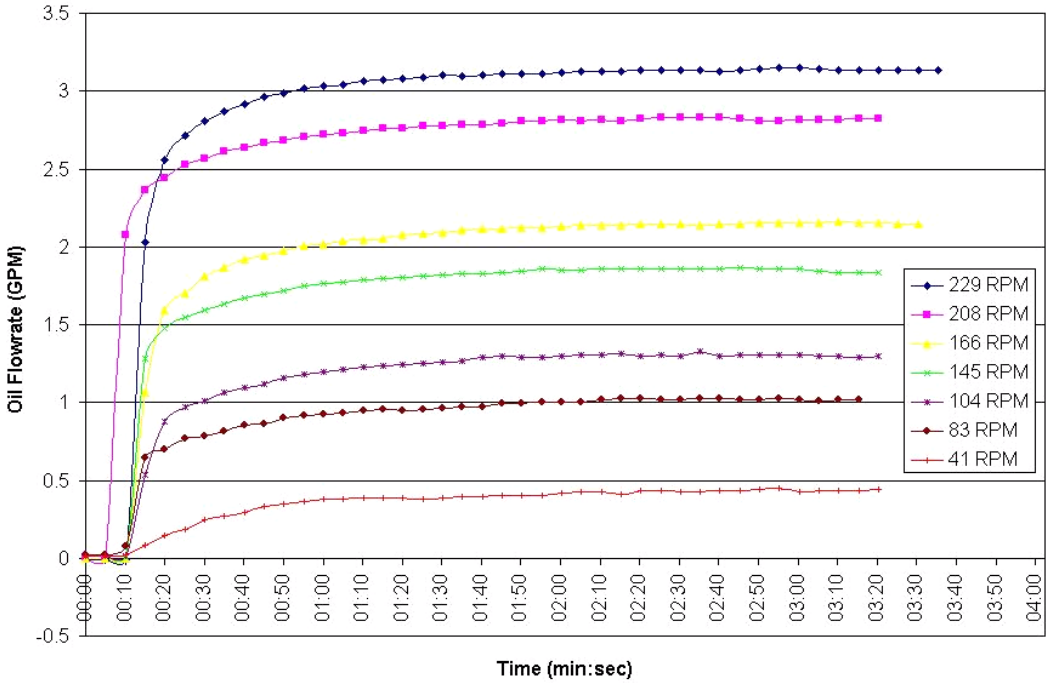

Figure 8. Pump calibration: oil flow rate as a function of time for the ½-inch straight tube for each of the pump operating speeds used. Data are extracted from video frames during stable flow, typically after approximately 90 seconds of operation.

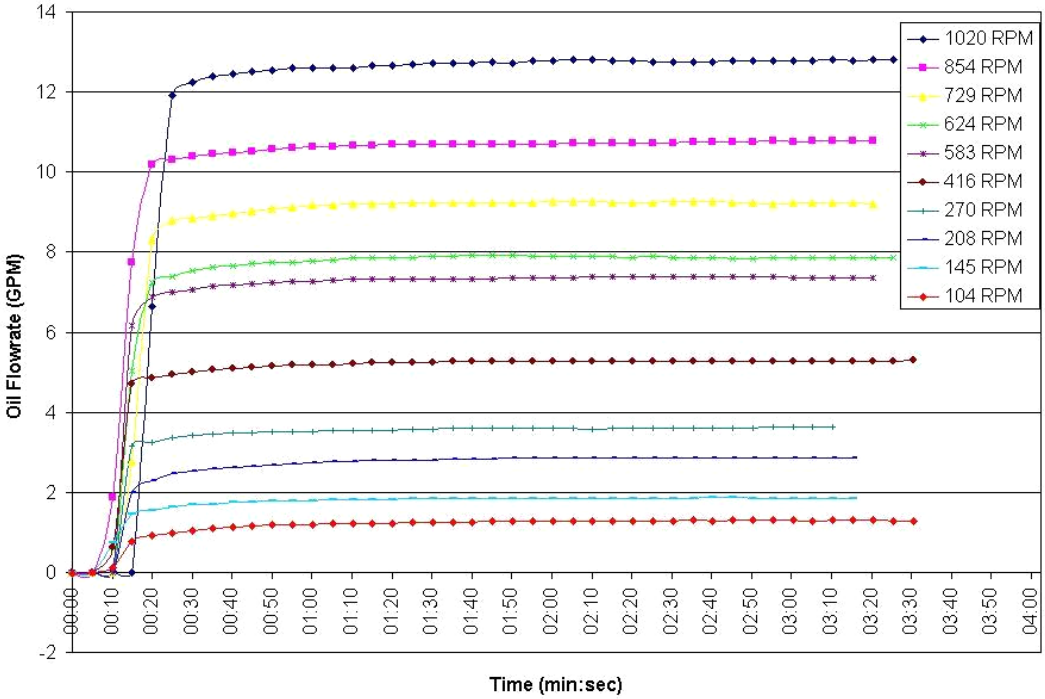

Figure 9. Pump calibration: oil flow rate as a function of time for the 1-inch straight tube for each of the pump operating speeds used. Data are extracted from video frames during stable flow, typically after approximately 90 seconds of operation.

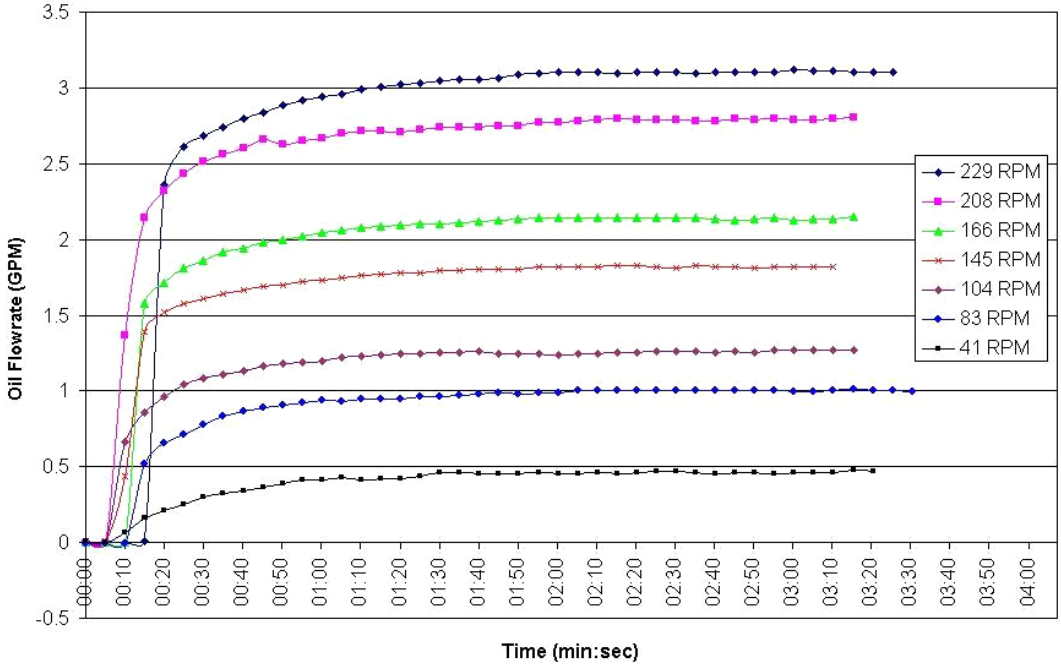

Figure 10. Pump calibration: oil flow rate as a function of time for the ½-inch J-tube for each of the pump operating speeds used. Data are extracted from video frames during stable flow, typically after approximately 90 seconds of operation.

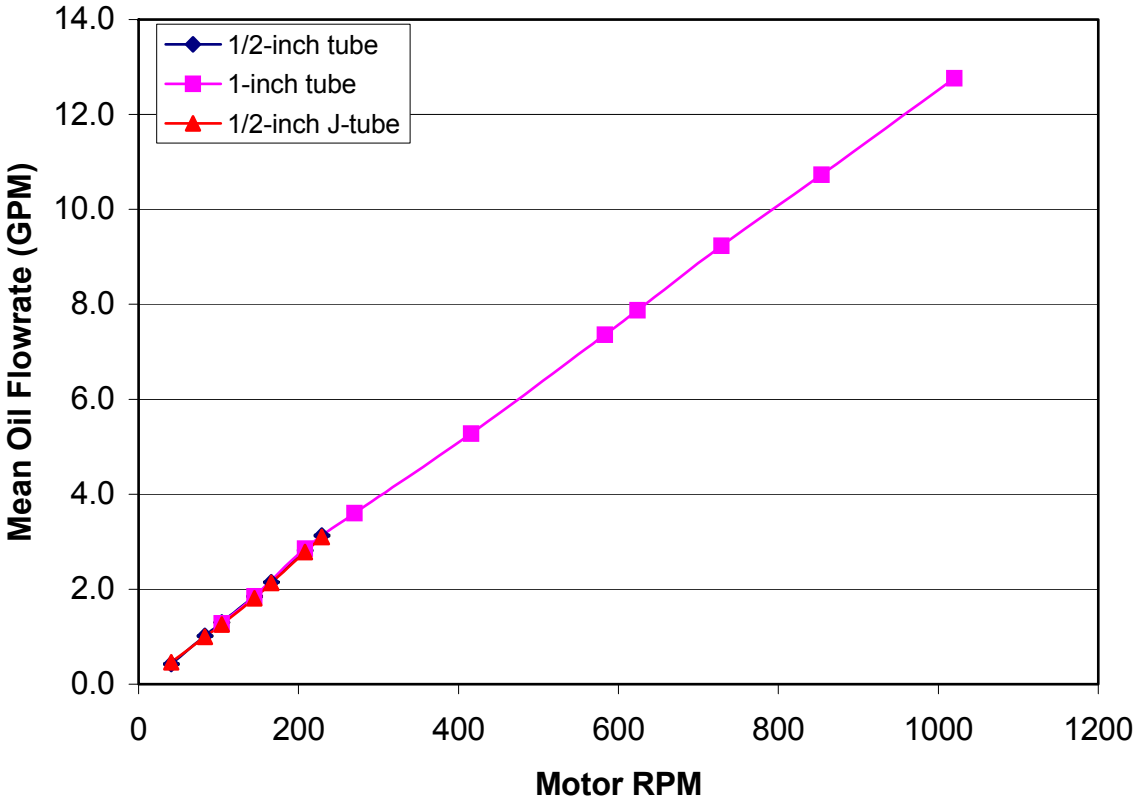

Figure 11. Pump calibration: oil flow rate as a function of motor RPM for the three injection tubes.

Simulant Liquids

Table 8 delineates the liquids used in the oil-brine injection hydrodynamics experiment and their relevant properties. In these initial experiments, simulant liquids are used instead of the actual liquids present in an SPR cavern. The reason for this is that crude oil and brine have significant issues (e.g., flammability, corrosion, vapors, and disposal) that make their use undesirable for initial experiments. Crude oil and brine will be examined in subsequent experiments.

Silicon oil (Dow Corning 200® Fluid, 5 cSt) and unsaturated sodium nitrate solution offer several additional advantages over crude oil and brine for the initial experiments. Most importantly, the hydrodynamic properties of the simulant liquids at laboratory conditions are similar to the hydrodynamic properties of the actual liquids at cavern conditions, as shown in Table 2. Neither liquid has difficulties associated with flammability, corrosion, vapors, or disposal. Furthermore, both liquids are transparent under ordinary conditions: slightly unsaturated sodium nitrate is used to avoid opacity from thermally induced nucleation of crystals, and, if necessary, the oil can accept a red dye to improve its visibility.

Table 8. Properties for SPR cavern and laboratory experiment. Handbook values used for properties (Weast, 1973).

Quantity	Symbol	Cavern	Experiment
Oil	"oil", subscript *o*	crude oil	Dow Corning 200 silicon oil
Brine	"brine", subscript *b*	sat. sodium chloride	unsat. sodium nitrate
Oil mass density	ρ_o	850 kg/m^3	913 kg/m^3 at 25 ^{o}C
Oil viscosity	μ_o	0.0040 kg/(m·s) ± 50%	0.0046 kg/(m·s) at 25 ^{o}C
Brine mass density	ρ_b	1200 kg/m^3	1244 kg/m^3 at 25 ^{o}C
Brine viscosity	μ_b	0.0015 kg/(m·s)	0.0017 kg/(m·s) at 25 ^{o}C
Interfacial tension	σ	0.05 J/m^2 ± 60%	0.059 J/m^2 at 20 ^{o}C
Gravitational accel.	g	9.81 m/s^2	9.79 m/s^2

Optical Measurements

Image-processing techniques are applied to determine the penetration depth of the oil jet, the width of the oil plume as it rises from the injection location to the oil-brine interface, and the interface deflection when the oil-brine plume impinges on it. A Canon Optura mini digital video camera is used to record images of the plume exiting the injection pipe. A Hitachi Color CCD Model KP-C553 is used to record images of the oil/brine interface. The two camera feeds are connected through a Videonics MXPro digital video mixer to a JVC SVHS video recorder. The video mixer allows the images from both cameras to be combined on a single split-screen video frame. The cameras record video at the standard digital video rate of 29.97 frames per second.

Figures 12 through 14 show images of the oil jet for each of the three injection tubes over a range of oil injection velocities. The oil is easily distinguished from the sodium nitrate solution, and the jet penetration, the plume width, and the interface deflection can all be observed straightforwardly. Extracting data from such images is automated using ImagePro® image-processing software (Media Cybernetics, Inc., Silver Spring, MD) to find the interfaces and track them automatically.

Oil with Sudan Red III red dye (Pylam Products Co., Inc., Tempe, AZ, 85281) was used in early experiments. However, the dye tends to leave a particulate residue at the oil-brine interface, and it is difficult to select a dye concentration that permits both the plume and the oil-brine interface to be visualized simultaneously. Therefore, a new lighting method is developed that allows visualization of the oil plume when injected into the brine with no dye added to either liquid. This method involves placing a black background behind the plume and illuminating the plume with uniform white light. With this method, the undyed plume appears white while the undyed brine appears transparent, so there is no need to dye the oil. This illumination method has also been extended to enable visualization of the oil-brine interface. The photos in Figures 12 through 14 are taken using the new method and show a vertically-split-screen view of the jet and the interface for each of the three different tubes tested.

Image Analysis

The images were acquired with slightly different magnifications, so the image processing was calibrated for each analysis using the following parameters:

Images with 0.5 inch pipe: 1 inch = 52 pixels
Images with 1.0 inch pipe: 1 inch = 40 pixels
Images with 0.5 inch J-tube: 1 inch = 50 pixels
Background ~ Black, Plume ~ White

Due to the wide variations in the plume width, length and contrast, an accurate measurement could not be made for every frame in a sequence. For example, in some frames, the right edge of the plume fell outside of the black background and was therefore not visible. In other images the plume edges consisted of several very small bubbles and the software could not identify a definite edge. Also, at some flow rates, extreme bursts sent the bottom of the plume below the camera's field of view. These errors were in only a few of the several thousand frames analyzed for each injection tube and flow condition, so such errors are considered negligible. In some images, a buildup of foam around the interface prevented the accurate measuring of the maximum interface penetration.

In most cases, when a correct value was not determined, the value recorded was negative, or much higher than a significant portion of data just before and just after the point in question. For example, when measuring the maximum plume width for the ½-inch pipe at 229 RPM, some values came out negative. This was because a right edge could not be detected. The right edge (0) minus the left edge (a value greater than 0) resulted in a negative number. These values were not included in the statistical (mean and standard deviation) results.

Analyzing line profile plots of several images from each run provided the "pre-determined" values needed to find plume edges and maxima.

To obtain the plume penetration distance, a thick (rectangular) vertical line profile was used in ImagePro® to measure the standard deviation of each row of pixels through the plume. The bottom of the plume was indicated by the standard deviation dropping below a threshold value. This point was detected and converted to a distance in inches from the tip of the nozzle.

The maximum plume width was determined using a thick (rectangular) horizontal line profile in ImagePro® and calculating the standard deviation. The analysis software scans the image from left to right. The far left edge of the plume was indicated by the standard deviation exceeding a pre-determined threshold value. Similarly, the far right edge of the plume was indicated by the standard deviation dropping below a pre-determined threshold value. The difference between the two extreme edges yielded the maximum plume width. In some frames, the right edge was not detected because the instantaneous edge of the plume extended beyond the edge of the black background. These values were not included in the statistical (mean and standard deviation) results.

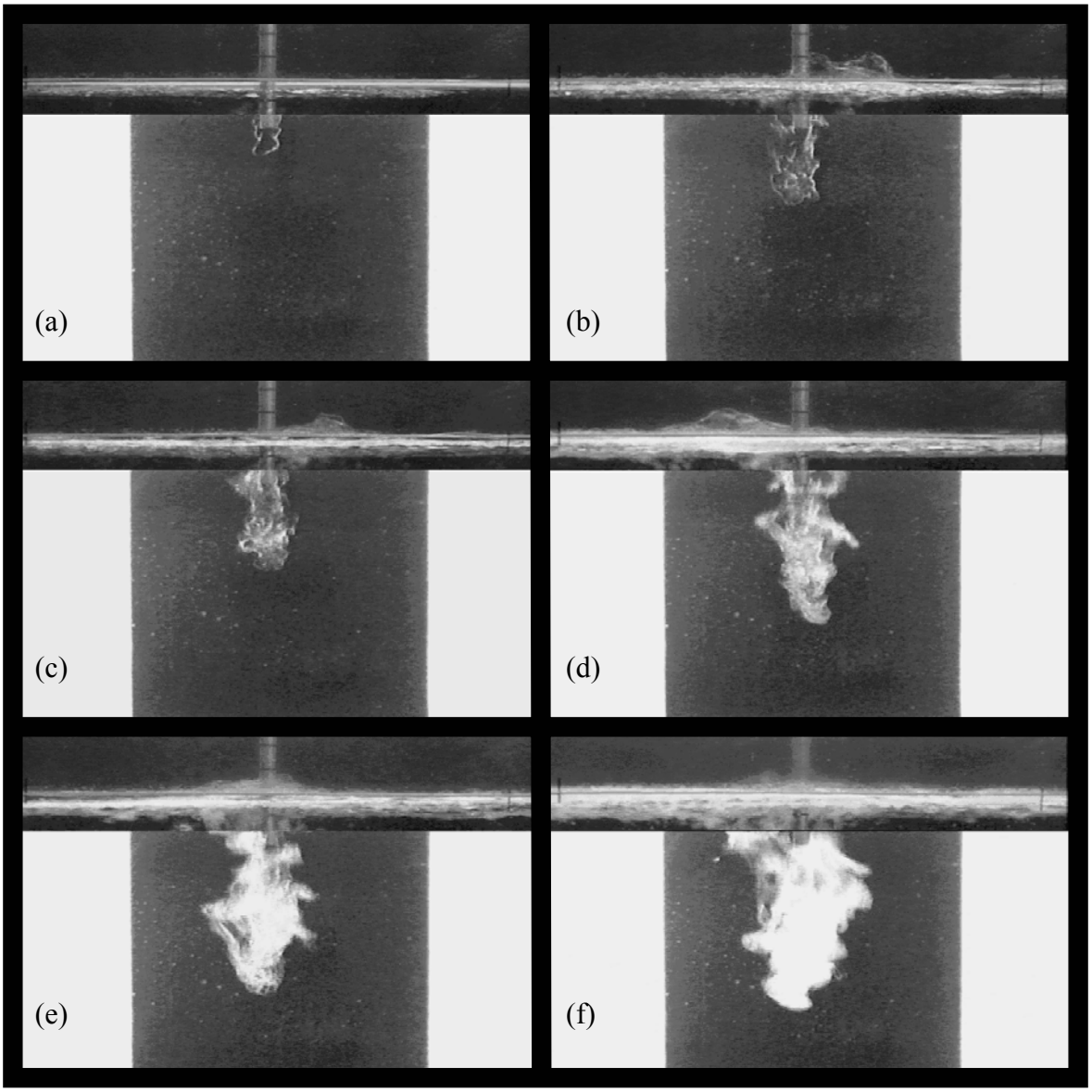

Figure 12. Photographs of oil injection with the ½-inch straight tube at velocities of (a) 0.24 m/s, (b) 0.58 m/s, (c) 0.74 m/s, (d) 1.05 m/s, (e) 1.22 m/s, and (f) 1.78 m/s. These are split screen views showing the plume and interface simultaneously; there is a 24-inch section of the vessel between the tube end and the interface not included in these images.

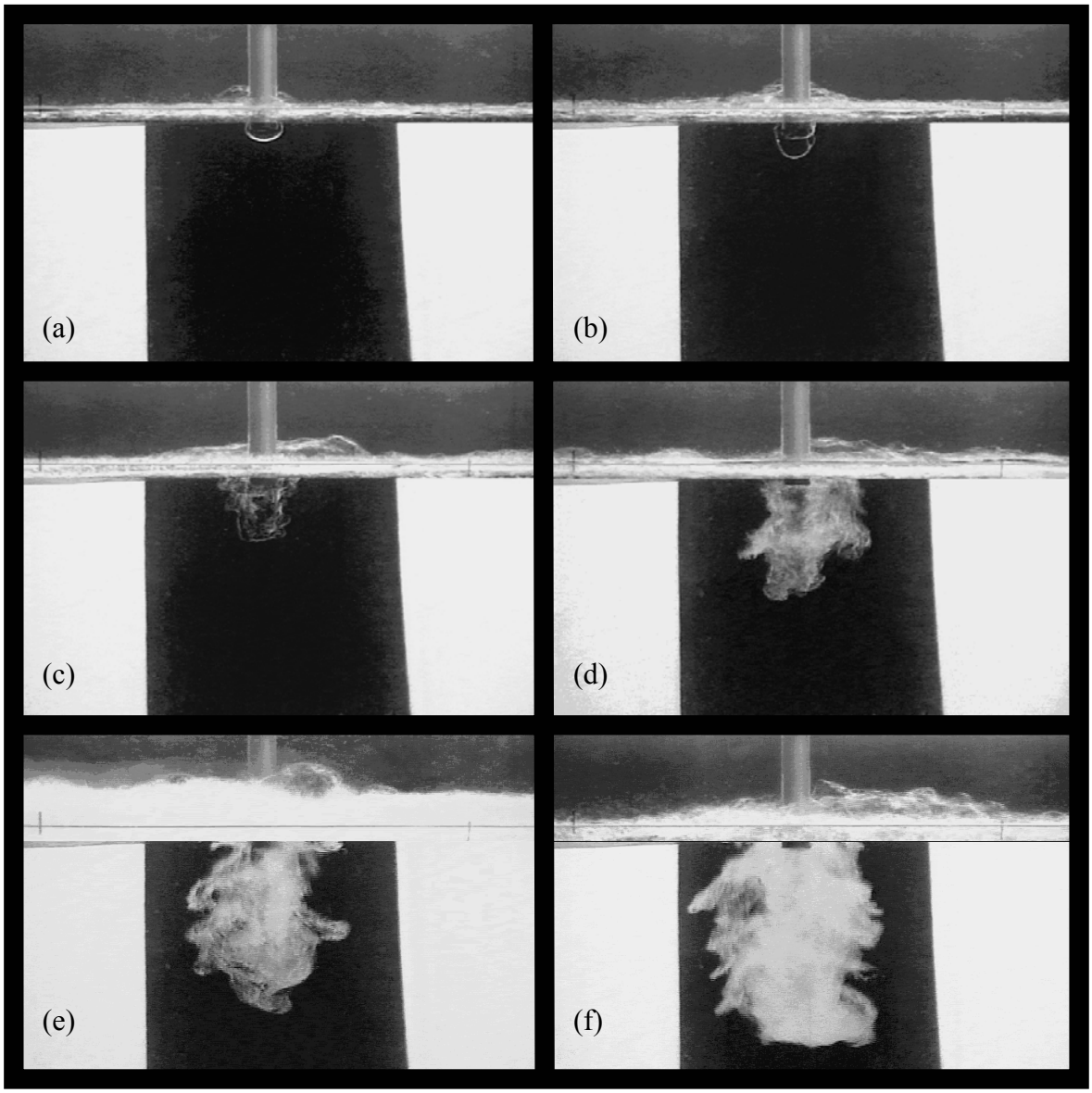

Figure 13. Photographs of oil injection with the 1-inch straight tube at velocities of (a) 0.17 m/s, (b) 0.25 m/s, (c) 0.49 m/s, (d) 1.0 m/s, (e) 1.25 m/s, and (f) 1.72 m/s. These are split screen views showing the plume and interface simultaneously; there is a 48-inch section of the vessel between the tube end and the interface not included in these images.

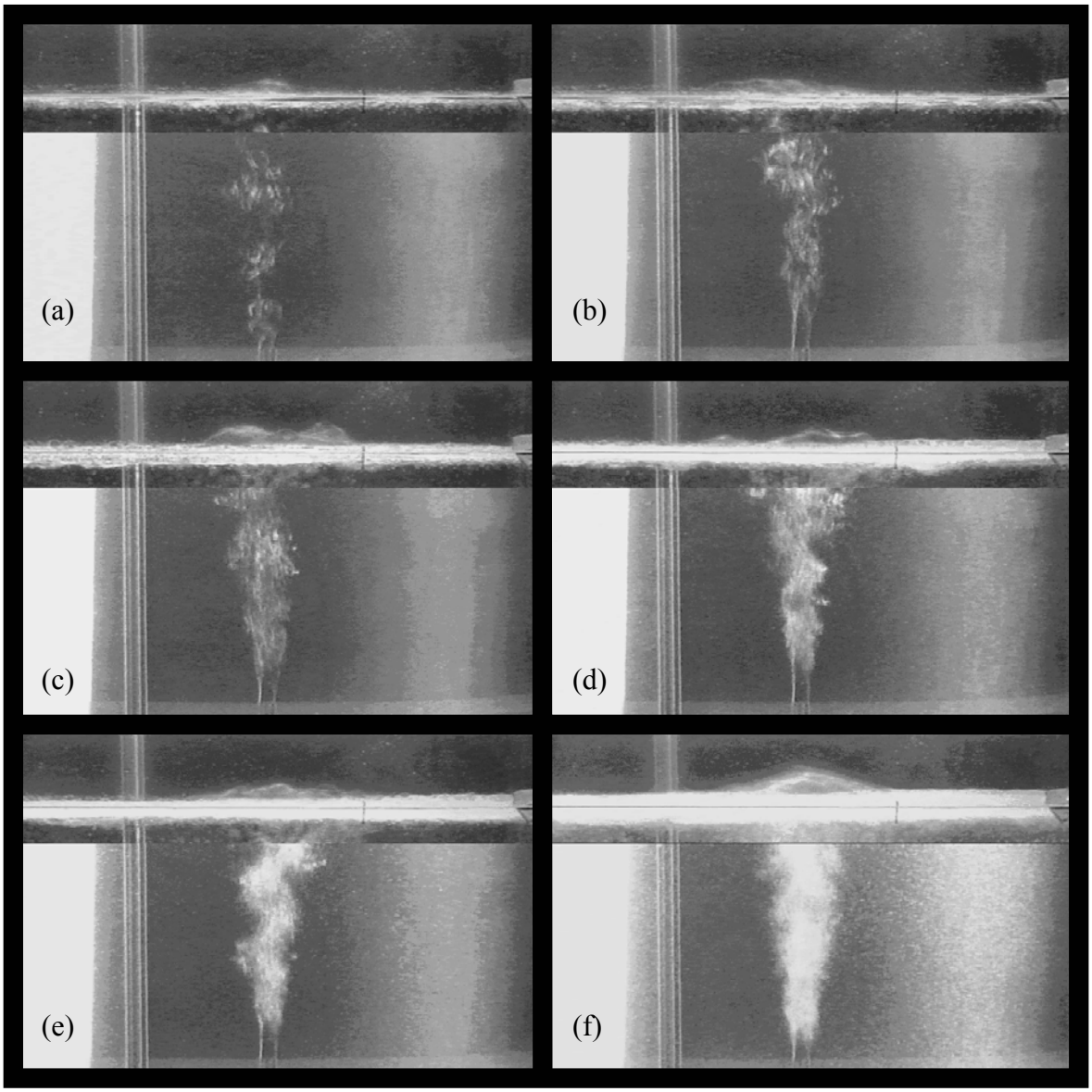

Figure 14. Photographs of oil injection with the ½-inch J-tube at velocities of (a) 0.26 m/s, (b) 0.56 m/s, (c) 0.71 m/s, (d) 1.03 m/s, (e) 1.21 m/s, and (f) 1.76 m/s. The downward portion of the J-tube is visible at the left in each image. These are split screen views showing the plume and interface simultaneously; there is a 24-inch section of the vessel between the tube end and the interface not included in these images.

RESULTS

Jet Penetration

Figures 15 through 18 present data extracted from video images of the oil plume during the ½-inch and 1-inch injection tube test series. The J-tube runs had zero penetration depth since the buoyant jet was injected upward. The time traces in Figure 15 and 17 demonstrate the unsteady nature of this flow. The range of fluctuations is indicated by the bars in Figures 16 and 18 which show ± one standard deviation of the jet penetration length. Figures 16 and 18 show that Equations 1 and 3 overpredict the penetration length for the ½-inch injection tube but Equation 1 gives a good prediction for the 1-inch injection tube. Adding a virtual origin term (allowing jet formation to begin at a location other than the tube exit) improved the prediction for the ½-inch tube for low to nominal injection flow rates but could not capture the rollover seen in Figure 16 at high injection flow rates. However, it is not clear why the ½-inch tube data roll over at higher flow rates. The data for the 1-inch injection tube are thought to be better than for the ½-inch tube since the scaling works out better.

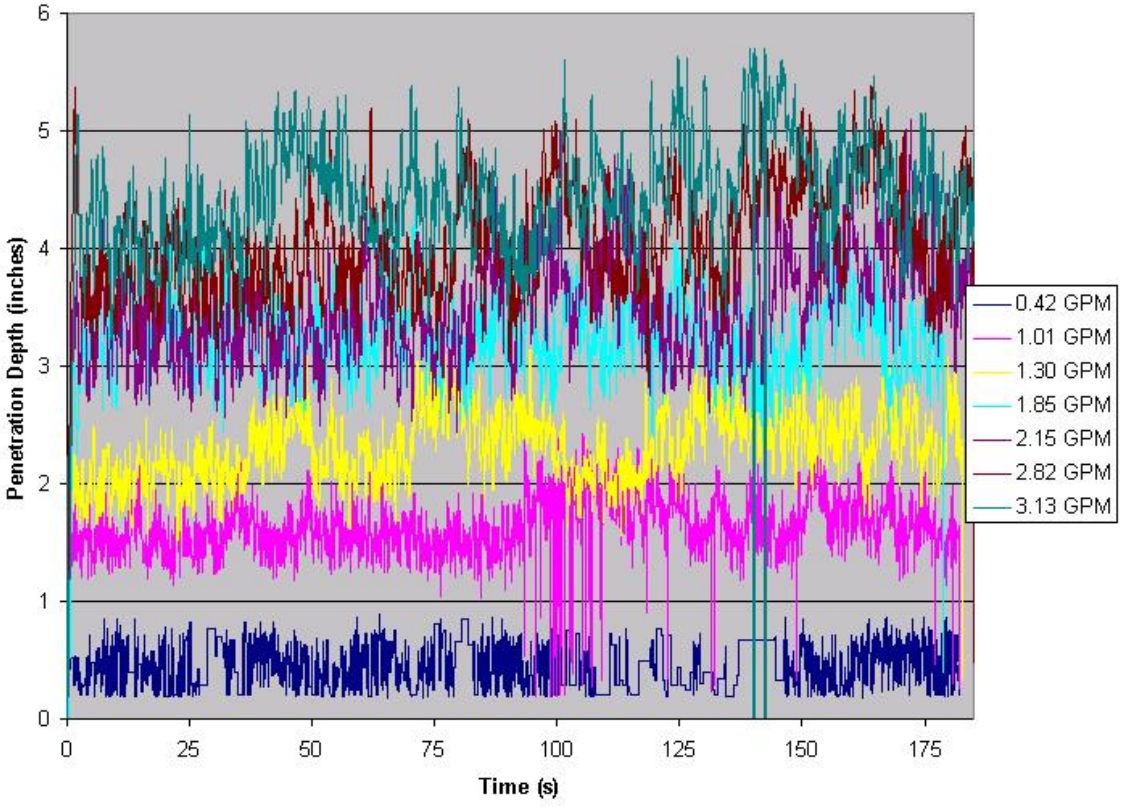

Figure 15. Time traces of jet penetration depth for the ½-inch straight tube.

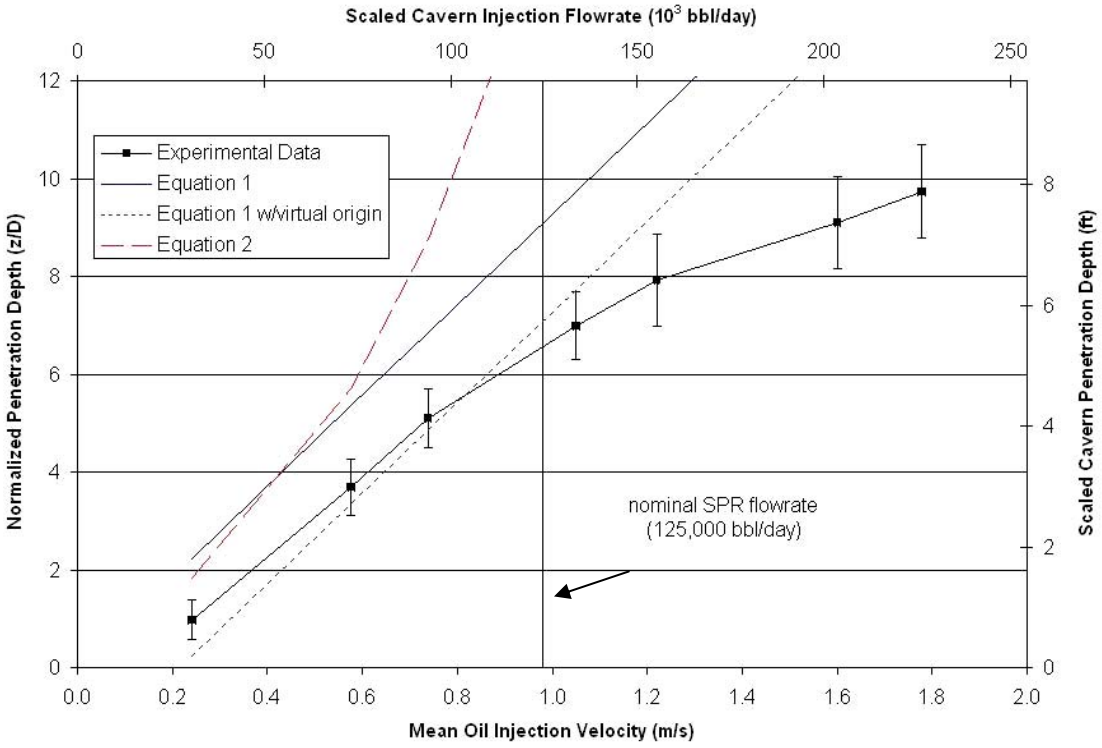

Figure 16. Penetration depth as a function of oil flow rate for the ½-inch straight tube. Cavern flow rate and penetration depth are scaled from laboratory data. Bars indicate ± one standard deviation of the penetration depth.

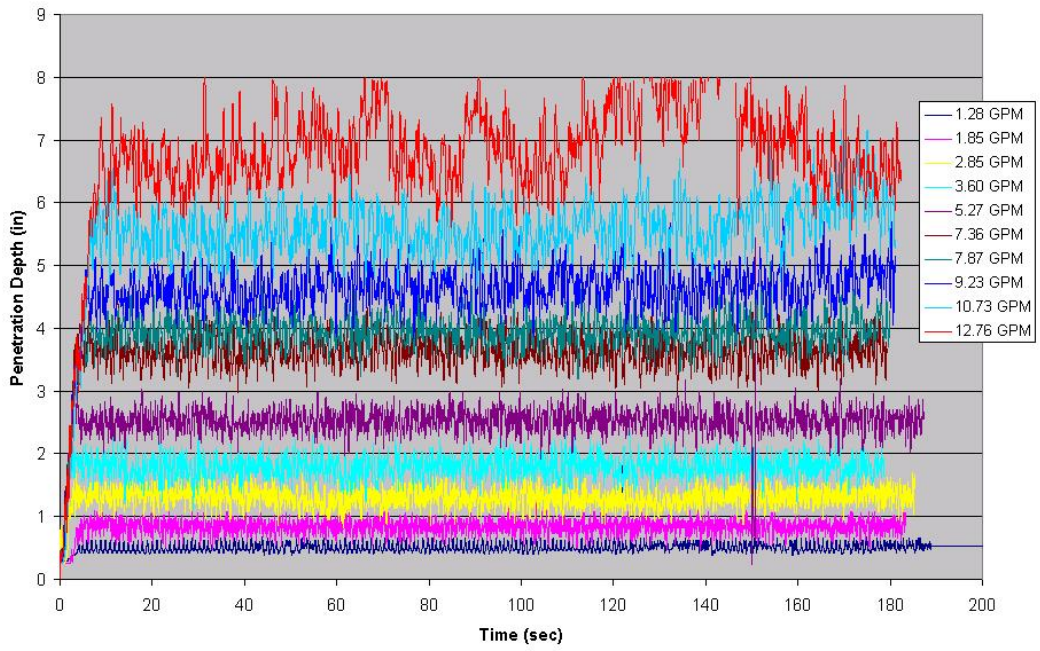

Figure 17. Time traces of plume penetration depth for the 1-inch straight tube.

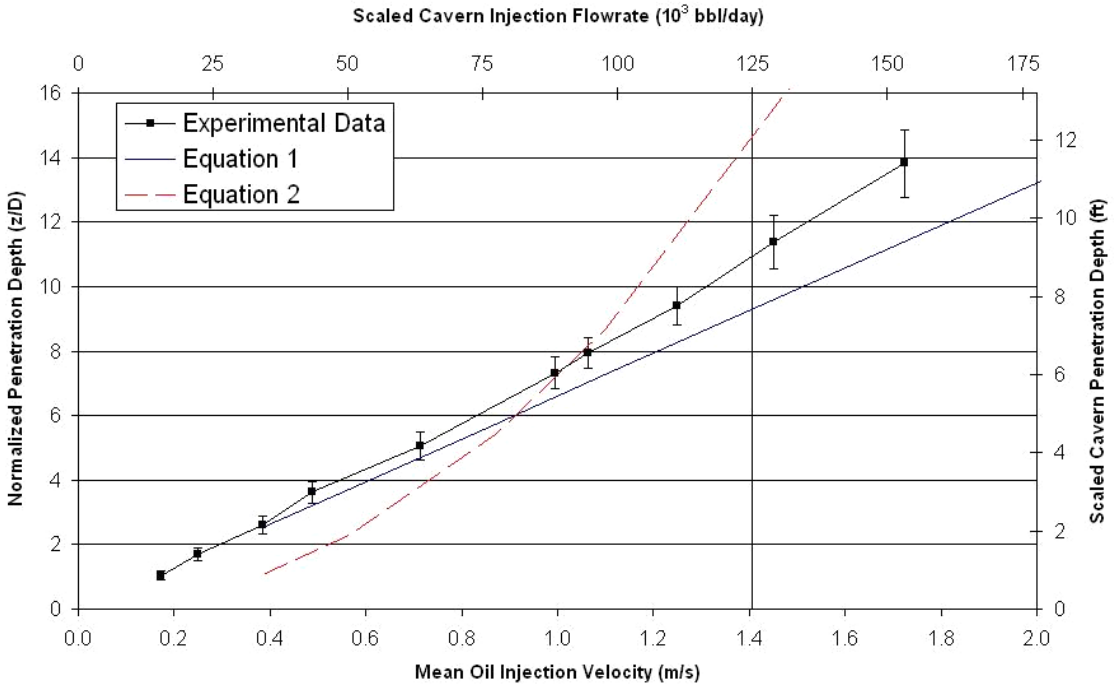

Figure 18. Penetration depth as a function of oil flow rate for the 1-inch straight tube. Bars indicate ± one standard deviation of the penetration depth.

Jet Width

Figures 19 through 21 present data extracted from video images of the plume width during each test series. Because these are split-screen images showing the jet exit and the interface only, the jet width values shown here are not the maximum in the flow (expected to occur at the oil-brine interface since the rising plume continuously grows by entrainment of brine) but rather the maximum width in the lower image, i.e., between the injection tube exit and the penetration depth for the downward-facing straight tubes and within the first 12 tube diameters downstream of the tube exit for the upward-facing J-tube. The flow is unsteady, and the jet width varied over wide ranges; an indication of the extent is given by the ± one standard deviation bars in Figures 19 through 21. As expected, the J-tube yielded a much narrower plume since the flow was directed upward, unlike the downward-oriented straight tube cases where the plume had to reverse direction, leading to a much wider effective plume area.

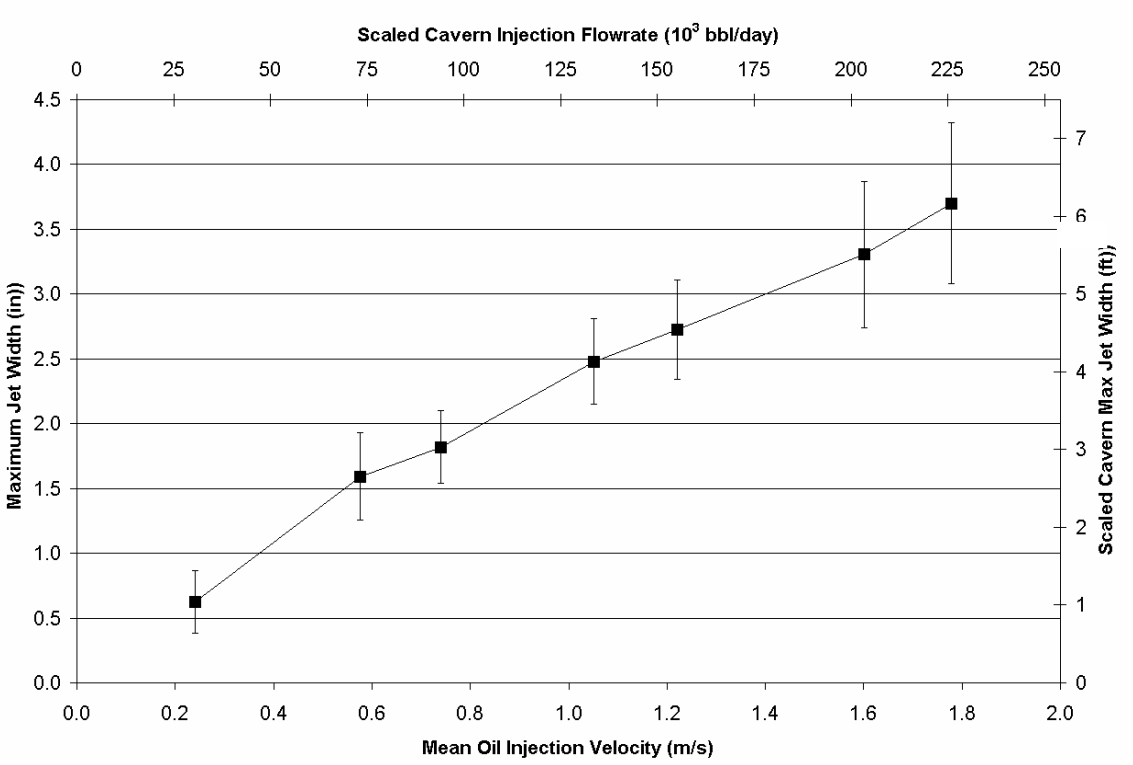

Figure 19. Maximum plume width from the tube end to the penetration depth for the ½-inch straight tube. Bars indicate ± one standard deviation of the jet width.

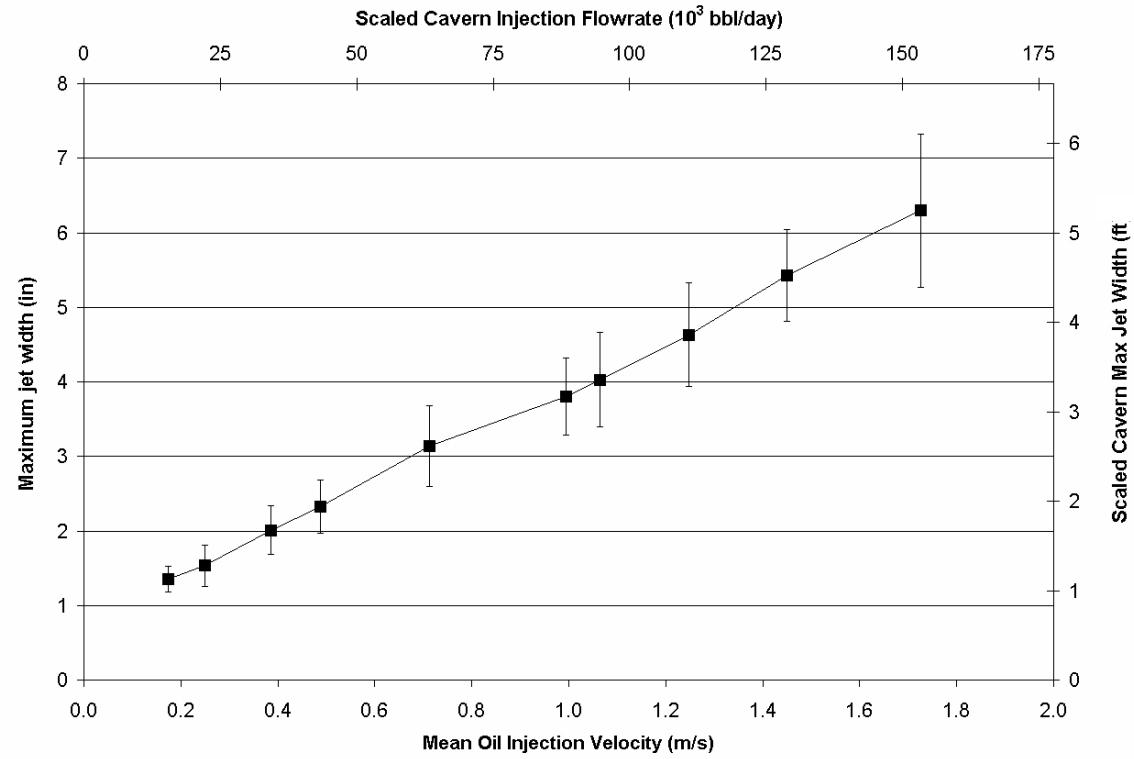

Figure 20. Maximum plume width from the tube end to the penetration depth for the 1-inch straight tube. Bars indicate ± one standard deviation of the jet width.

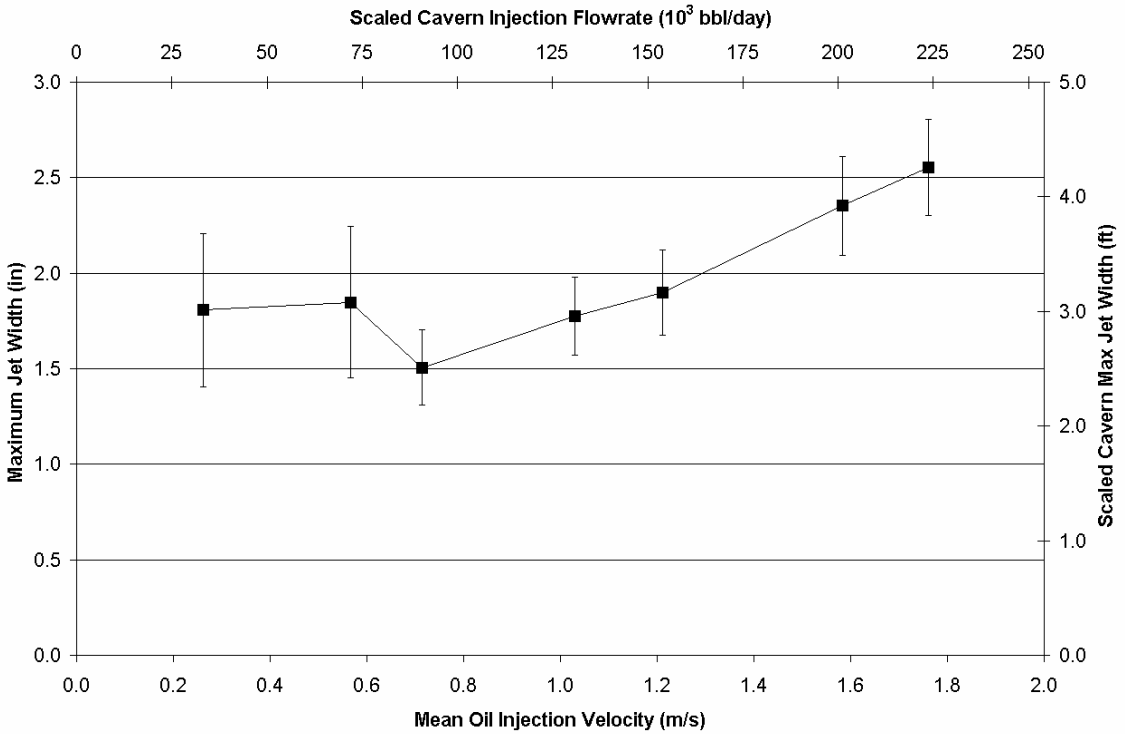

Figure 21. Maximum plume width from the tube end to the 12-diameter region (pointed upwards) for the ½-inch J-tube. Bars indicate ± one standard deviation of the jet width.

Interface Disturbance

Figures 22 through 24 present data extracted from video images of the interface deflection during each test series. The interface deflection was measured using image processing; however, foam buildup after several minutes of run time led to high uncertainty for the higher flow rate cases. Again, the flow is unsteady and the interface deflection varied over wide ranges; an indication of the extent is given by the ± one standard deviation error bars in Figures 22 through 24. Larger surface deflections were caused by the narrower plume emitted from the J-tube. Although velocity was not measured in these experiments, the J-tube plume was clearly faster than those emitted from the downward-oriented tubes. This is evident in Figures 12 through 14. These results indicate that oil injection tube modifications could inhibit emulsion formation by limiting the contact between the oil and the brine.

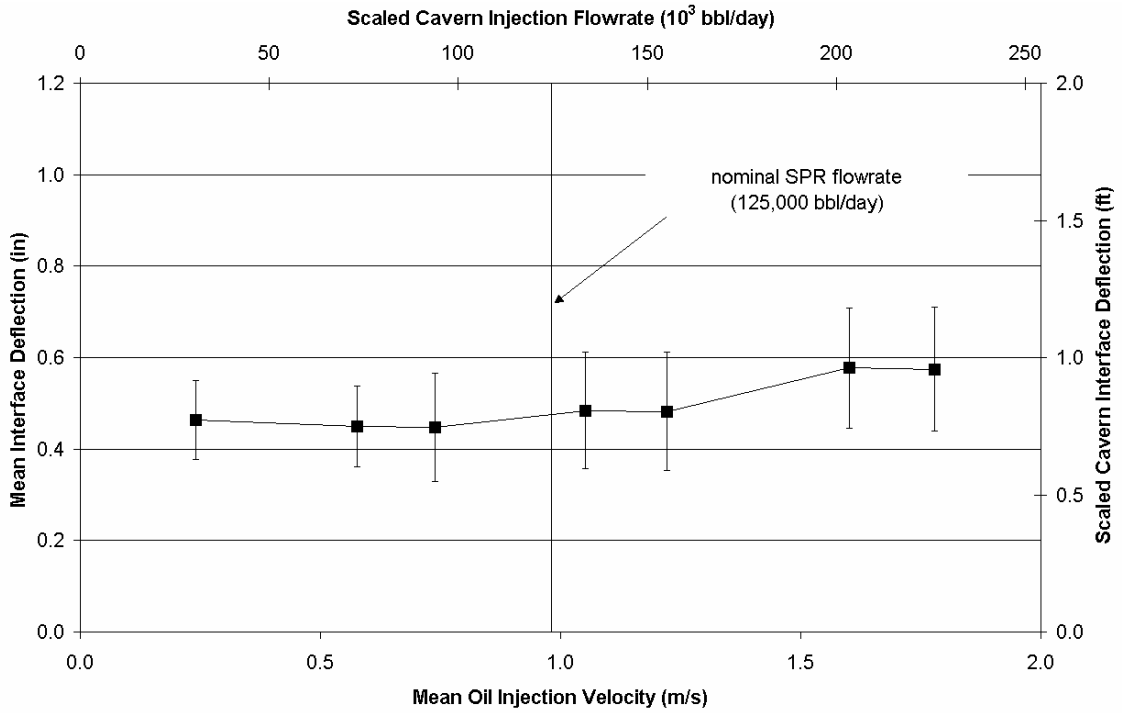

Figure 22. Mean interface disturbance for the ½-inch straight tube. Bars indicate ± one standard deviation of the interface deflection. Cavern flow rate and penetration depth are scaled from laboratory data.

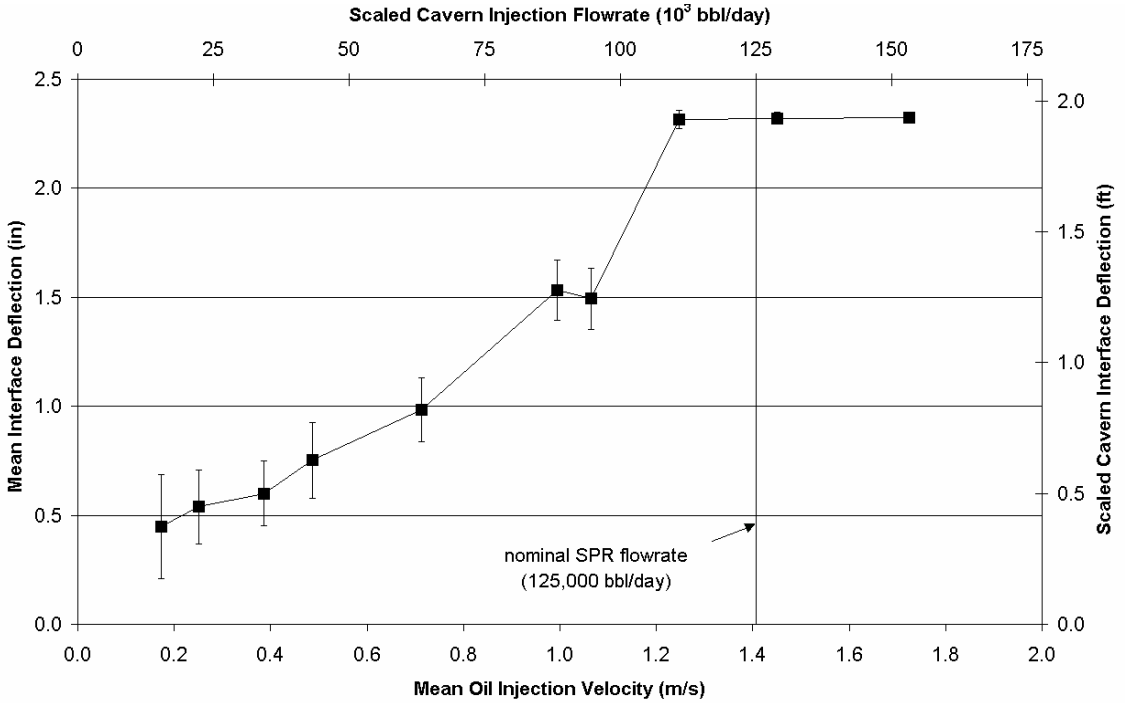

Figure 23. Mean interface disturbance for the 1-inch straight tube. Values for two highest velocities are unclear due to foam formation at interface. Bars indicate ± one standard deviation of the interface deflection. Cavern flow rate and penetration depth are scaled from laboratory data.

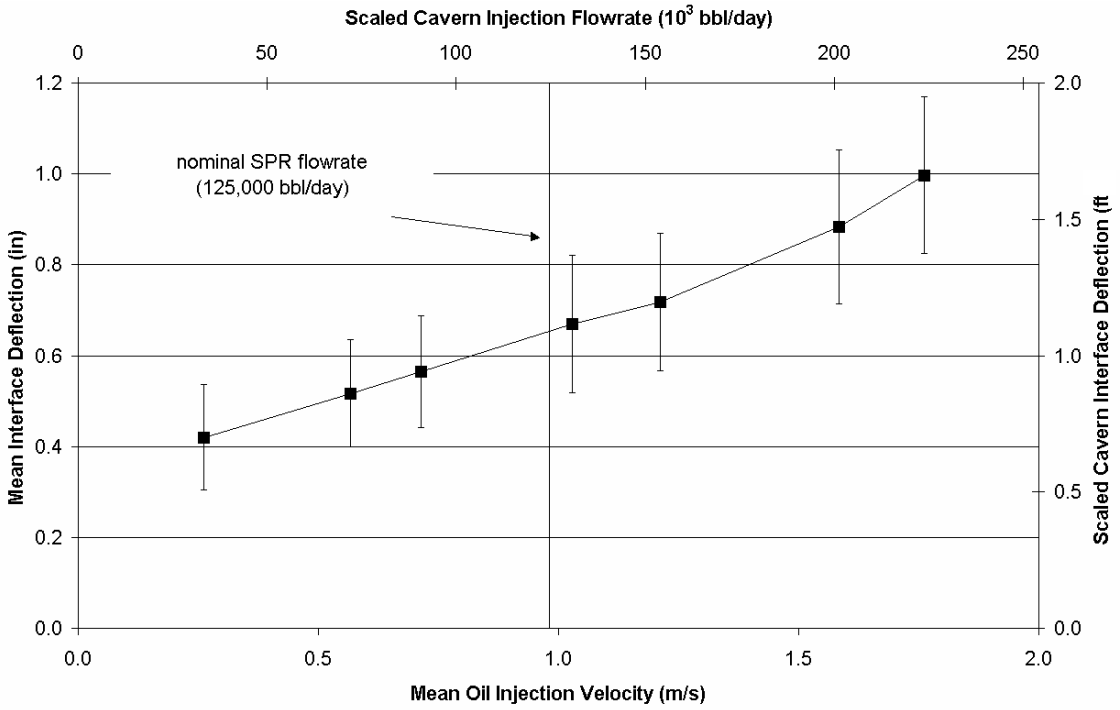

Figure 24. Mean interface disturbance for the ½-inch J-tube. Bars indicate ± one standard deviation of the interface deflection. Cavern flow rate and penetration depth are scaled from laboratory data.

CONCLUSIONS

A laboratory experiment has been designed and fabricated to examine the hydrodynamics involved with injecting oil into brine. The vessel is a reduced-scale version of the actual injection region in a cavern of the Strategic Petroleum Reserve (SPR). Simulant liquids are used in this phase of the experiment, and the actual liquids (crude oil and brine) will be used in the later phases. Information about the oil-jet penetration depth was compared to previously developed scaling relations and will be used to design the oil-brine interface emulsion experiment.

The measured penetration depths are shallow, as predicted by the penetration depth models, in agreement with the assumption that the flow is buoyancy-dominated, rather than momentum-dominated. The turbulent penetration depth model provided a good estimate of the measured values for the 1-inch injection tube but overpredicted the penetration depth for the ½-inch injection tube. Adding a virtual origin term improved the prediction for the ½-inch tube for low to nominal injection flow rates but could not capture the rollover at high injection flow rates. Since the 1-inch tube data are considered better in terms of scaling, we recommend use of the turbulent penetration depth model (Equation 1) to predict plume penetration distance in SPR caverns.

As expected, the J-tube yielded a much narrower plume since the flow was directed upward, unlike the downward-oriented straight tube cases where the plume had to reverse direction, leading to a much wider effective plume area. Larger surface deflections were caused by the narrower plume emitted from the J-tube. Although velocity was not measured in these experiments, the video data showed that the J-tube plume was faster than those emitted from the

downward-oriented tubes. These results indicate that oil injection tube modifications could inhibit emulsion formation by limiting the contact between the oil and the brine.

FUTURE WORK

There are two major aspects of the upcoming work. The first is to repeat key flow visualization experiments using real fluids from SPR caverns. These experiments will provide a check on the data acquired here and an indicator of its applicability for real cavern fluids. Since the real oil is an opaque black color, visualization of the interface deflection will probably not be done with the real fluids. However, measurement of the jet penetration length and the jet width will be made. Comparison of those results with the ones presented in this report will be made. If the measurable jet characteristics are in good agreement, then the interface deflection values measured with simulant fluids are expected to be applicable to the real fluid case. The second aspect is to use real oil, brine, and sludge from SPR caverns to determine the stability of the emulsion formed by oil droplet interactions with brine in the presence of sludge. This will be done by running the experiment with the 1-inch pipe, essentially used as a droplet injector allowing oil droplets to rise to the oil-sludge-brine interface. The resulting emulsion, or thickened sludge layer, will be sampled as a function of time. Samples will be analyzed using Karl Fischer titration or equivalent to determine the water content. Sampling will be done at several locations across the thickness of the thickened sludge layer.

NOMENCLATURE

a	parameter in similarity solution
A	aspect ratio
b	parameter in similarity solution
Bo	Bond number
c	parameter in similarity solution
d	parameter in similarity solution
D_1	injection pipe inner diameter
D_2	injection pipe outer diameter
D_3	cavern diameter
D_T	turbulent diffusivity
d_{max}	maximum stable droplet diameter
d_{min}	minimum unstable droplet diameter
d_e	effective droplet diameter
F_1	buoyancy flow rate
Fr	Froude number
g	gravitational acceleration
h_m	penetration depth (frictionless)
L_1	injection pipe length below oil-brine interface
L_2	injection pipe exit height above cavern bottom
L_3	interface depth below cavern top
L_4	cavern bottom-to-top height = $L_1 + L_2 + L_3$
Mo	Morton number
Q_1	oil volumetric flow rate
Re	Reynolds number
T	temperature
U_1	oil average velocity at pipe end
w	vertical velocity component
z_m	penetration depth (turbulent)

Greek Symbols

γ	density ratio
ε_o	volume fraction
κ	viscosity ratio
μ	absolute viscosity
ν	kinematic viscosity
ρ	density
σ	oil-brine interfacial tension
τ	shear stress

Subscripts

b	brine phase
o	oil phase

REFERENCES

Clift, R., Grace, J. R., and Weber, M. E., 1978, *Bubbles, Drops, and Particles* (Academic Press, New York), especially pp. 26-27, 341-344.

Davis, R. H., and Acrivos, A., 1985, "Sedimentation of Noncolloidal Particles at Low Reynolds Numbers," *Annual Reviews of Fluid Mechanics* **17**, 91-118.

O'Hern, T. J., and Torczynski, J. R., 2000, "Proposal to Investigate Flow Issues During the Reintroduction of Oil into SPR Caverns," Sandia internal memorandum to T. E. Hinkebein, August 1.

Torczynski, J. R., and O'Hern, T. J., 2001, "Analysis and Design of Strategic Petroleum Reserve (SPR) Oil-Reintroduction Experiment," Sandia internal memorandum to T. E. Hinkebein, May 24.

Turner, J. S., 1979, *Buoyancy Effects in Fluids* (Cambridge University Press, Cambridge), especially Chapters 1 and 6, Section 6.1.

Weast, R. C., 1973, *Handbook of Chemistry and Physics* (CRC Press, Cleveland, OH), especially pp. D-219 and D-222.

DISTRIBUTION

Internal

1	MS 0750	6118	T. E. Hinkebein
1	MS 0735	6115	R. E. Finley
1	MS 0719	6142	S. W. Webb
1	MS 0828	9100	T. C. Bickel
1	MS 0824	9110	W. L. Hermina
1	MS 0834	9112	M. R. Prairie
1	MS 0834	9112	R. O. Cote
1	MS 0834	9112	J. N. Castañeda
1	MS 0834	9112	J. Barney
1	MS 0834	9112	J. Oelfke
5	MS 0834	9112	T. J. O'Hern
1	MS 0834	9112	S. M. Trujillo
1	MS 0826	9113	S. N. Kempka
5	MS 0826	9113	J. R. Torczynski
1	MS 0834	9114	J. E. Johannes
1	MS 0836	9117	R. O. Griffith
1	MS 9018	8945-1	Central Technical Files
2	MS 0899	9616	Technical Library

External:

5 Professor Kim A. Shollenberger
Mechanical Engineering Department
California Polytechnic State University
San Luis Obispo, CA 93407

SPR

CD only Wayne Elias
FE 4431
DOE SPR PMO
900 Commerce Road East
New Orleans, LA 70123